國 立 交 通 大 學

電信工程學系碩士班

碩 士 論 文

多天線頻域正交多工系統之
頻率, 資料與通道的合併估測

Joint Frequency, Data and Channel Estimation
for MIMO OFDM Systems

研究生：呂子逸

指導教授：蘇育德 博士

中 華 民 國 九 十 四 年 七 月

多天線頻域正交多工系統之

頻率, 資料與通道的合併估測

Joint Frequency, Data and Channel Estimation

for MIMO OFDM Systems

研 究 生：呂子逸   Student : Tzu-I Lu

指導教授：蘇育德 博士   Advisor : Dr. Yu T. Su

國 立 交 通 大 學

電信工程學系碩士班

碩 士 論 文

A Thesis Submitted to
Department of Communications Engineering
College of Electrical Engineering and Computer Science
National Chiao Tung University
In Partial Fulfillment of the Requirements
For the Degree of Master of Science
In
Communications Engineering
July 2005

Hsinchu, Taiwan, Repubic of China

中華民國九十四年七月

多天線頻域正交多工系統之

頻率,資料與通道的合併估測

研究生：呂子逸　　　　　　　　　　　　指導教授：蘇育德 博士

國立交通大學電信工程學系碩士班

摘要

我們探討在頻域正交多工(OFDM)系統中合併頻率、資料與通道的估測的可行性。由於載波頻率偏移(Carrier Frequency Offset, CFO)所造成的頻域信號的載波間干擾(Inter-Carrier Interference, ICI)與複徑通道所引起在時間軸上符碼間干擾(Inter-Symbol Interference, ISI)有類似的數學模式，後者的許多已知解決方案，如最大可能性序列估測(Maximum Likelihood Sequence Estimation, MLSE)，便可用來解決前者。然而，不同於傳統的 MLSE 可直接套用 Viterbi 演算法，我們面對的是含有未知參數（不確定性）的籬柵(Trellis)圖。我們採用遞迴式估合併檢測與估計(Iterative Joint Detection and Estimation)的原則來解決。

首先，我們針對單天線 (SISO) 系統的狀況來設計，並且針對效能及複雜度等主要課題提出改進方案。我們討論了利用接收端視窗(Windowing)的等效濾波及刪除較小載波干擾的鄰頻等降低籬柵狀態(trellis state)數目的方法的可行性以降低演算法的複雜度。我們也探討採用不同通道估測法對系統效能的影響。接著，我們將這套遞迴式估合併檢測與估計演算法推展到多天線(MIMO)的系統。

為研究我們所提出演算法的效能及各系統及通道參數的效益，我們採取 IEEE802.11n 標準，Task Group'n'synchronization（或簡稱 TGn Sync）所提出來的傳輸信號架構為基礎來做電腦模擬。所得到的數值結果顯示，無論是 SISO 或 MIMO 環境，我們的解決方案都能提供令人滿意的表現。

Joint Frequency, Data and Channel Estimation for MIMO OFDM Systems

Student : Tzu-I Lu   Advisor : Yu T. Su

Department of Communications Engineering

National Chiao Tung University

Abstract

We consider the problem of joint carrier frequency offset (CFO)/channel estimation and data detection for orthogonal frequency-division multiplexing (OFDM) systems. An iterative approach is employed. The iteration procedure consists of an inner CFO/data estimation loop and an outer CFO/data-channel estimation loop. We first discuss the single-input single-output (SISO) case and then extend to a multiple-input multiple-output (MIMO) scenario. Drawing an analogy between the inter-carrier interference corrupted frequency domain waveform and the inter-symbol interference limited time domain waveform, we apply maximum likelihood sequence estimation scheme to detect the data sequence in the presence of residual CFO. Related algorithms either for reducing the implementation complexity like the trellis state number or for improving the overall performance such as receiver time domain windowing and refined channel estimates are presented. Computer simulation results based on a candidate IEEE 802.11n standard–the Tgn Sync (Task Group n) proposal–are given to predict the performance of the proposed algorithms.

誌謝

　　研究所的兩年中，非常感謝我的指導教授：蘇育德老師。在他循循善誘的教導中，使我能夠一步一步地將本論文完成。做研究的過程中，陳彥志學長以及洪佳君等同學都不吝情給予極大的幫助；學弟妹們更熱情的贊助電腦儀器以供模擬之用，令我好生感動。

　　在心理的調適與建設上，女友柔嫚，好友士瑋、政龍於平時即不斷的鼓勵我，並且調劑我的生活情趣，讓我擁有積極向上的力量以渡過研究中的瓶頸。海賊王動畫也是我舒壓的方式之一，主角魯飛的毅力更是我最好的典範。

　　此外，特別感謝聯發科技公司的贊助以及指導，使得為期一年的研究計畫得以順利進行。最後，對我的父母親以及家人致上十分的謝意，感謝他們給予我良好的環境，讓我的求學生涯無後顧之憂。

Contents

List of Figures

Chapter 1

Introduction

The main idea behind the orthogonal frequency division multiplexing (OFDM) waveform is to split a data block into multiple parallel sub-blocks so that each of them is transmitted by distinct orthogonal subcarriers. The orthogonality between those transmitted sub-streams is ensured by choosing a proper subcarrier spacing. By inserting a cyclic prefix in the (parallel-to-serial) combined time-domain signal before it is transmitted via the main carrier, intersymbol interference (ISI) caused by a multipath channel can be eliminated at the receiving end if the corresponding cyclic prefix part in each OFDM frame is removed.

The cyclic prefix (also known as the guard interval) of an OFDM block is a copy of the last portion of the original block and if the maximum channel path delay is smaller than the guard interval duration, the received time-domain waveform will be a weighted sum of various delayed version of the transmitted blocks. Deleting the cyclic prefix, each data-bearing subcarrier experiences only flat fading. Such an arrangement enables an OFDM-based system to overcome frequency selective fading in broadband wireless transmission and is the major reason for its current popularity.

Due to its effectiveness, OFDM has been selected as standards for various wireless applications, such as digital audio broadcasting (DAB) [1], digital video broadcasting (DVB) [2]-[4], high performance local area networks (HIPERLAND/2) [5], and IEEE

802.11a wireless local area networks (WLAN) [6]. OFDM also plays an important role in future standards, such as IEEE 802.11n [7] [8], 802.16e, and 802.20, some of them are likely to include the Multiple Input Multiple Output (MIMO) option for capacity enhancement. We will give a brief introduction in Section A.

With all its merits, OFDM, unfortunately, is far more sensitive to synchronization errors, especially the carrier frequency offset (CFO), than single carrier systems. CFO is primarily caused by relative movement or channel-induced Doppler shifts and instabilities of and mismatch between transmitter and receiver oscillators [9]. In high dynamic environment, the received waveform is likely to encounter large Doppler shifts by antipodal frequencies. Residual CFO results in inter-carrier interference (ICI) among subcarriers due to the loss of orthogonality and will bring about serious performance degradation. Whence it is highly desirable to reduce the sensitivity of OFDM systems to CFO of any kind.

There have been a multitude of proposals for CFO compensation. But most of them require pilot symbols or training sequences [10], which lowers the effective data rate. Blind techniques that operate in the time domain [11] often require observation over a number of OFDM symbols, and are not suitable for tracking time-varying CFO. Decision-directed modifications of some pilot-assisted CFO estimation are more promising but require good initial estimate. On the other hand, the ultimate goal of a receiver is the detection of the transmitted data stream and, as the detection of OFDM signals takes place in the frequency domain, channel estimation must be obtained before data detection commences. Conventional OFDM channel estimators, however, are derived under a zero or negligible CFO assumption. We therefore face the dilemma of channel estimation in the presence of CFO and CFO estimation without pilots or reliable decisions.

It is thus the goal of this investigation to develop feasible solutions to the above joint estimation and detection problem. We adopt an iterative approach for joint

CFO/channel estimation, tracking and data detection. To simply our problem, we shall assume that the initial CFO is to be less than one half of the subcarrier spacing. Drawing an analogy between the ICI effect on a frequency domain signal and the ISI effect on a time domain signal, we can easily apply the maximum likelihood sequence estimation (MLSE) technique to detect the data stream in the presence of ICI, assuming known CFO.

Chapter 2 begins with the simple scenario that no channel estimation is needed. Assuming an initial CFO estimate we use the Viterbi algorithm to obtain an estimate of the transmitted data sequence. The CFO estimate is then refined and updated by considering the new information provided by the estimated data sequence. The updated CFO, in turn, is used to modify the trellis for a new run of Viterbi detection. The iteration procedure stops when convergence is achieved (usually 2 or 3 iterations is enough).

When frequency selective fading is present, channel estimate is needed for data detection. Because the channel estimation requires CFO information our iterative procedure will consist of two loops in which the joint CFO/data estimation constitute an inner loop while the joint channel and CFO/data estimation procedure forms the outer loop. More specifically, the inner loop follows the same iterative procedure described in the above paragraph and, when a convergence is detected, the information is passed to the channel estimator to produce a new estimate. The new channel estimate is then used by the inner loop for another run of joint CFO/data estimation. Simulation results indicate that both inner and outer loops converge very rapidly. The complexity is mostly associated with the Viterbi search and channel estimator. The former has to do with the ICI range, i.e., the number of neighboring subcarriers that interfere the desired subcarrier while the latter depends on the algorithm used.

In Chapter 3, we suggest the use of Nyquist windowing in time domain to suppress the ICI effect and reduce the number of trellis states through truncation and decision

3

feedback [22]. We also study the effectiveness of an improved channel estimator. It is shown that the receiver complexity is greatly reduced without significant performance degradation.

Chapter 4 extends our investigation to a MIMO environment and finally, Chapter 5 summarizes the main results and suggests topics for further studies. In all simulations, BPSK is used as the subcarrier modulation. For reference purpose, we provide a brief description of the IEEE 802.11n standard proposed by the TGn Sync group in Appendix A.

Chapter 2

Joint Frequency Data and Channel Estimation for SISO-OFDM Systems

In a real-world scenario, received OFDM signals often suffer from residual frequency offsets, caused by oscillator instabilities and relative movement-induced Doppler spread, resulting in inter-carrier interference (ICI) among subcarriers. It is desirable to reduce the sensitivity of OFDM to carrier frequency offsets .

2.1 Joint CFO Estimation and Data Detection

2.1.1 System model in AWGN channels

Shown in **Fig. 2.1** is a block diagram of an OFDM transmitter. The mapper converts input data stream into complex valued constellation points, according to the selected constellation, e.g., BPSK, QAM. The complex valued data sequence is parallel-to-serial converted before being used to modulate multiple carriers via an inverse discrete Fourier transformation (usually through the inverse fast Fourier transform, IFFT).

Each OFDM symbol has a "useful interval" of length T_u and a cyclic prefix (CP)(or "guard interval") with duration T_g; see **Fig. 2.2**. The CP is a periodical repetition of the useful interval so that precise timing recovery is not needed as long as the discrete Fourier transform frame of the receiver starts within the guard interval. In order to protect the
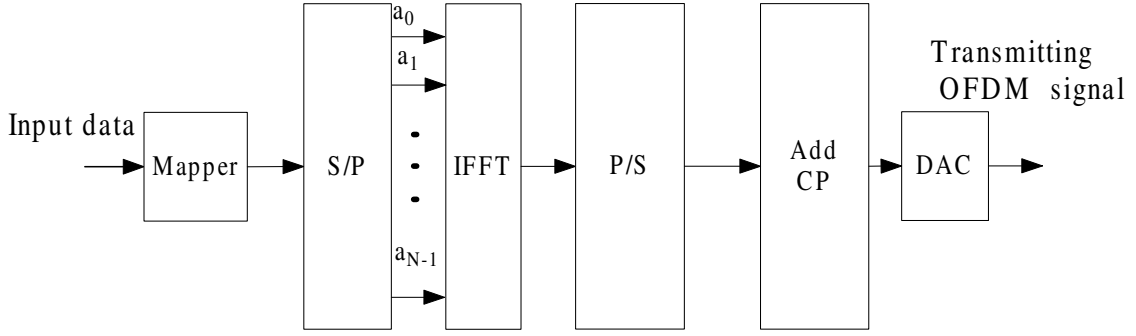
Figure 2.1: Block diagram of an OFDM modulator.

OFDM signal against inter-symbol interference (ISI), the CP is set longer than the maximum channel memory, $T_g/T_u < 0.25$ being a practical value. The baseband signal is modulated by a Nyquist signaling pulse, up-converted to the radio frequency (RF) and then transmitted through the channel. At the receiver, the signal is down-converted
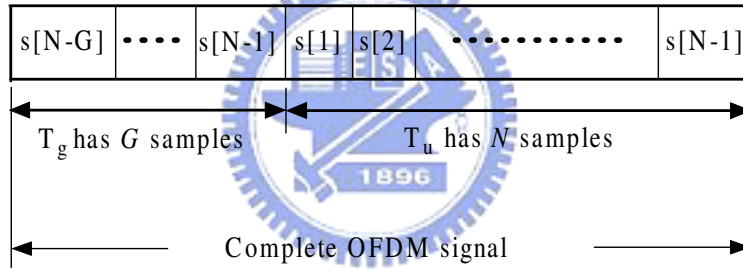
Figure 2.2: Structure of complete OFDM signal with the guard period (interval).

to the intermediate frequency (IF) and then demodulated (**Fig. 2.3**). After removing the cyclic prefix, the signal part of the received time-domain baseband waveform can be expressed as

$$s[n] = \frac{1}{N} \sum_{k=0}^{N-1} a_k e^{j2\pi nk/N} e^{j2\pi f_e n/N} \tag{2.1}$$

where,

- a_k represents the symbol carried by the kth subcarrier. The i.i.d. data sequence $\{a_k\}$ is such that $E[a_k] = 0$ and $E[|a_k|^2] = 1$.

6
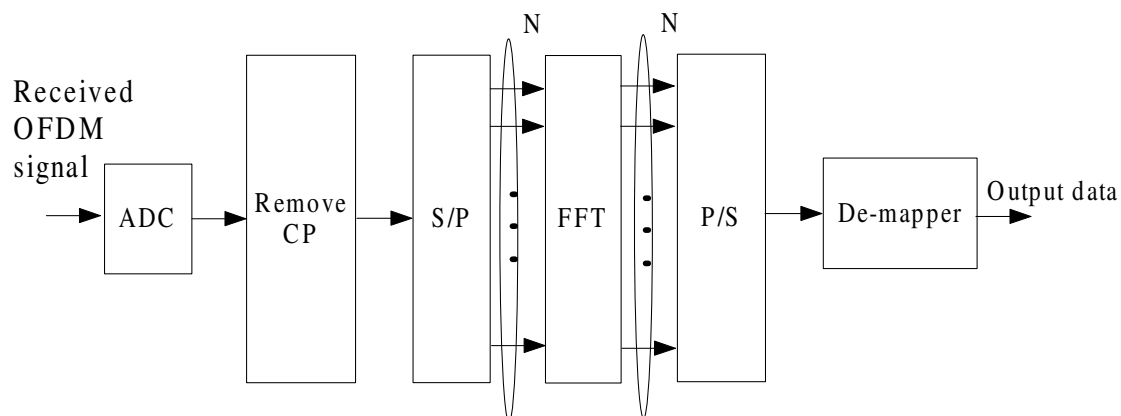
Figure 2.3: Block diagram of a typical OFDM demodulator.

- N = the number of subcarriers.

- f_e is CFO normalized by the intercarrier spacing $f_t = 1/T_u$ and T_u is an OFDM symbol period (without cyclic prefix).

This time domain signal is then passed through a serial-to-parallel convertor and then an FFT demodulator. Assuming an AWGN channel, the signal at the FFT output becomes

$$r_k = \frac{1}{N} \sum_{n=0}^{N-1} s[n]w[n]e^{-j2\pi nk/N} + n_k \tag{2.2}$$

where $w[n]$ represents the receiver pulse shaping function and n_k is additive white Gaussian noise (AWGN). Plugging (2.1) into (2.2), the received signal can be written as

$$
\begin{aligned}
r_k &= \sum_{m=0}^{N-1} a_m \left\{ \frac{1}{N} \sum_{n=0}^{N-1} w[n]e^{-j2\pi n(k-m)/N} e^{j2\pi f_e n/N} \right\} + n_k \\
&= \sum_m a_m W_{k-m}^{f_e} + n_k \\
&= a_k W_0^{f_e} + \underbrace{\sum_{m \neq k} a_m W_{k-m}^{f_e}}_{ICI} + n_k \tag{2.3} \\
&= y_k(f_e, \mathbf{a}) + n_k \tag{2.4}
\end{aligned}
$$

where $W_k^{f_e} = \frac{1}{N} \sum_{n=0}^{N-1} w[n]e^{-j2\pi nk/N} e^{j2\pi f_e n/N}$

As shown in (2.3), the signal portion of r_k, can be viewed as the output of an ISI

7

channel driven by the input $\mathbf{a}$ with the channel response $W_k^{f_e}$,dependent upon the given CFO, f_e. The choice of the window function $w[n]$ affects the extent of ISI (actually the ICI in this case). To control the complexity of the estimator, the length of $W_k^{f_e}$ must be kept reasonably short. We will discuss how to choose pulse shaping function later in Section 3.1.

2.1.2 Joint frequency-data sequence estimation algorithm

With a proper window shaping, we can rewrite (2.3) as

$$r_k \approx a_k W_0^{f_e} + \sum_{m=k-L, m \neq k}^{m=k+L} a_m W_{k-m}^{f_e} + n_k \tag{2.5}$$

where L is usually less or equal than 2 for $|f_e| < 0.5$.

2.1.2.1 Data detection

Given $\hat{f}_e$, the data detection is equivalent to estimating the state of a discrete-time finite-state machine. The finite-state machine in this case is the equivalent discrete-time channel with coefficients $\{W_k^{\hat{f}_e}\}$ and its state at any instant in time is given by the $2 * L$ most recent inputs. Even though we have noncausal term in (2.5), we can add a delay function so that the resulting model is causal.

$$r_{k-L} \approx a_k W_{-L}^{\hat{f}_e} + a_{k-1} W_{-L+1}^{\hat{f}_e} + ... + a_{k-2L} W_L^{\hat{f}_e} + n_{k-L} \tag{2.6}$$

The state at time k is

$$S_k = (a_{k-1}, a_{k-2}, ..., a_{k-2L}) \tag{2.7}$$

If the information symbols are M-ary, the channel filter has M^{2L} states. Consequently, the channel is described by an M^{2L}-state trellis and the Viterbi algorithm may be used to determine the most probable path through the trellis.

2.1.2.2 CFO estimation
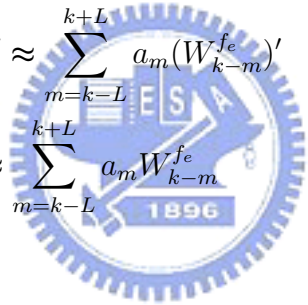
Given $\hat{\mathbf{a}}$ as well as $\mathbf{r}$, we can get a CFO estimate by finding f_e that minimizes the cost function

$$C(f_e) = \sum_k |r_k - y_k(f_e, \hat{\mathbf{a}})|^2 \tag{2.8}$$

The minimization of (2.8) is carried out base on a gradient descent search method as following:

$$
\begin{aligned}
\nabla_{f_e}(C(f_e)) &= \frac{\partial C}{\partial f_e} \\
&= \sum_k \left\{ -\mathbf{A} \cdot r_k^* - \mathbf{A}^* \cdot r_k + \mathbf{B} \cdot \mathbf{A}^* + \mathbf{A} \cdot \mathbf{B}^* \right\}
\end{aligned}
\tag{2.9}
$$

where $(\ )^*$ denote the complex conjugate and

$$
\begin{aligned}
\mathbf{A} &= \sum_m a_m (W_{k-m}^{f_e})' \approx \sum_{m=k-L}^{k+L} a_m (W_{k-m}^{f_e})' \qquad , (W_{k-m}^{f_e})' = \frac{\partial W_{k-m}^{f_e}}{\partial f_e} \\
\mathbf{B} &= \sum_m a_m W_{k-m}^{f_e} \approx \sum_{m=k-L}^{k+L} a_m W_{k-m}^{f_e}
\end{aligned}
\tag{2.10}
$$

A *learning rate u* is introduced to control the rate of change in each iteration

$$
\begin{aligned}
f_e^1 &\leftarrow f_e^0 - u * \nabla_{f_e}(C(f_e^0)) \\
f_e^2 &\leftarrow f_e^1 - u * \nabla_{f_e}(C(f_e^1)) \\
&\vdots \\
f_e^m &\leftarrow f_e^{m-1} - u * \nabla_{f_e}(C(f_e^{m-1}))
\end{aligned}
$$

When f_e^m reaches a stable value with very little jitter, which indicates that we have arrived at a minimum, the algorithm stops; see **Fig. 2.4**.

9
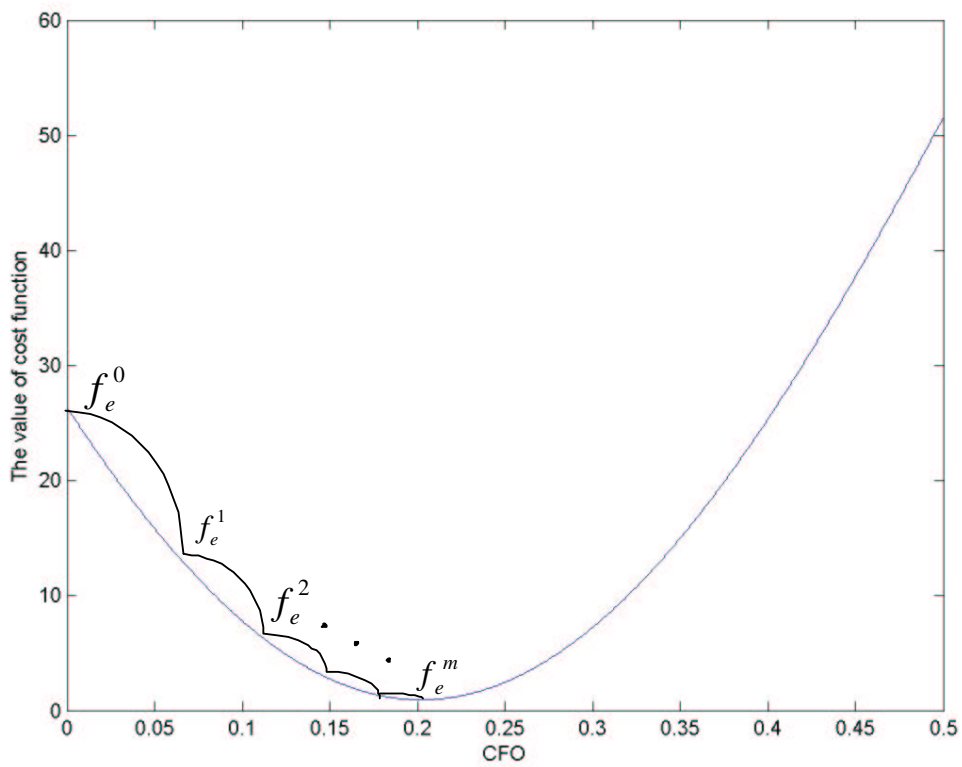
Figure 2.4: An example of cost value for CFO=0.2 without noise.

The joint frequency-data sequence (FD) estimation algorithm consists of the following steps:

A.1 (Frequency Estimate Initialization) Set the initial estimate $\hat{f}_e$ to zero.

A.2 (Starting the FD iteration loop) Using the CFO estimate $\hat{f}_e$, generate the corresponding frequency domain "channel response" $W_k^{f_e}$:

$$W_k^{f_e} = \frac{1}{K} \sum_{n=0}^{K-1} w[n] e^{-j2\pi n(k-m)/K} e^{j2\pi f_e n/K}$$

A.3 (Compute the tentative data estimate) Based on the observation baseband samples r, we run the Viterbi algorithm using the branch metric

$$\lambda_k = |r_k - y_k(\hat{f}_e, \mathbf{a})|^2$$

to obtain an estimate $\hat{\mathbf{a}}$ of the transmitted data sequence.

A.4 (Update the frequency estimate) Given $\hat{\mathbf{a}}$ from Step 3 as well as $\mathbf{r}$, we obtain a new CFO estimate by searching for f_e that minimizes the cost function

$$C = \sum_k |r_k - y_k(f_e, \hat{\mathbf{a}})|^2$$

A.5 (Convergence check and end of the FD loop) If the new CFO estimate is close enough to the previous estimate, i.e. absolute difference is less than 10^{-6}, then stop the iteration and release the most recent estimate; otherwise, go to Step 2.

Simulation shows that this algorithm usually converges within just two or three iterations.

2.2 Joint Estimator for Frequency-Selective Channels

2.2.1 System model for frequency-selective channels

For frequency-selective fading channels, we assume that the CP is longer than the channel impulse response whence there is no frequency domain self interference between

successive OFDM symbols. With such an assumption we can concentrate on a single OFDM symbol scenario. Let the signal part of the received signal be given by

$$s[n] = \frac{1}{N} \sum_{k=0}^{N-1} a_k H_k e^{j2\pi nk/N} e^{j2\pi f_e n/N} \tag{2.11}$$

where H_k is the channel response at k/T. After taking FFT, the received signal becomes

$$r_k = \frac{1}{N} \sum_{n=0}^{N-1} s[n]w[n]e^{-j2\pi nk/N} + n_k \tag{2.12}$$

Like the AWGN case, we have

$$
\begin{aligned}
r_k &= \sum_{m=0}^{N-1} a_m H_m W_{k-m}^{f_e} + n_k \\
&= y_k(f_e, \mathbf{a}, \mathbf{H}) + n_k
\end{aligned}
\tag{2.13}
$$

2.2.2 Joint frequency-data sequence-channel (FDC) estimation algorithm

The estimator proposed in the previous section cannot be applied directly to (2.13) because the channel response is unknown. However, assuming the data sequence and the CFO are known, the channel impulse response can be easily estimated.

2.2.2.1 Channel estimation

For every subcarrier n, the channel can be estimated as (using LS):

$$\hat{H}_n = \frac{1}{a_n}[(\mathbf{F}^H\mathbf{F})^{-1}\mathbf{F}^H\mathbf{r}]_n \ , \ n = 0, 1, ..., N-1 \tag{2.14}$$

where

$$\mathbf{F} = \begin{bmatrix} W_0^{f_e} & \cdots & W_{-N+1}^{f_e} \\ \vdots & \ddots & \vdots \\ W_{N-1}^{f_e} & \cdots & W_0^{f_e} \end{bmatrix}$$

$$\mathbf{r} = \begin{bmatrix} r_0 \\ r_1 \\ \vdots \\ r_{N-1} \end{bmatrix}$$

12

Based on this channel estimator and the joint CFO-data sequence estimator proposed in the previous section, we arrive at the following iterative joint CFO-data sequence-channel estimation algorithm.

B.1 (Channel estimate initialization) Let $\hat{H}_O$ to be the channel estimate from the previous OFDM symbol interval.

B.2 (FD iteration loop) Using this channel estimate, the CFO f_e and the symbol sequence $\mathbf{a}$ are estimated by the joint FD estimation algorithm described in the previous section.

B.3 (Channel estimate update) Compute a new channel estimate $\hat{H}_N$ using (2.14) based on the current estimates $\hat{f}_e$ and $\hat{\mathbf{a}}$.

B.4 (Convergence check for the channel estimate) If the new channel estimate $\hat{H}_N$ is close enough to the previous estimate, more specifically, if

$$\left| \frac{\hat{H}_N - \hat{H}_O}{\hat{H}_N} \right|^2 < 10^{-2}$$

then stop iteration and release the most recent estimates. If not, go to Step 2.

We plot the overall receiver structure in **Fig. 2.5**.
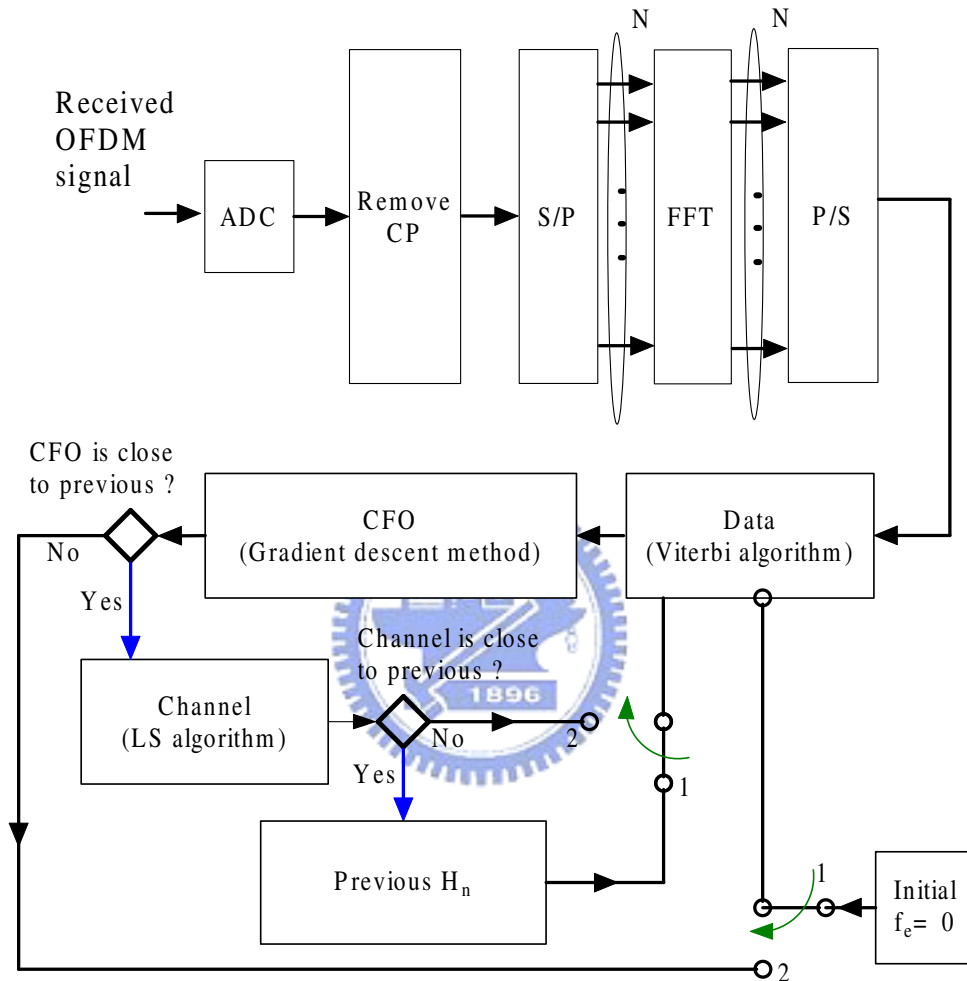
Figure 2.5: Illustrating the proposed iterative joint Frequency-Data Sequence-Channel (FDC) estimation algorithm". Initially, the switch is in position 1; and for the tracking mode it is moved to position 2; It stops when the new channel estimation is close enough to the previous estimate .

2.3 Numerical Experiments

The computer simulation results reported in this section are obtained by using a pilot and data format which are the same as the Tgn Sync 802.11n proposal (52 data tones and 4 pilot tones); see the Appendix. It is a slight modification of the IEEE 802.11a data format (48 data tones and 4 pilot tones).

From **Fig. 2.6** we can see that the proposed joint FD estimator gives good BER performance in AWGN channels. The mean squared estimation error (MSEE) performance of the frequency estimate for different f_e is plotted in **Fig. 2.7**, where SNR is defined as the ratio of the total transmit signal energy per bit to noise power density.

The frequency-selective fading channel is modelled as an linear FIR filter with impulse response given by

$$h(k) = \sum_{n=0}^{C_L-1} \alpha_n e^{-j\Phi} \delta(k - n) \qquad (2.15)$$

where Φ is uniformly distributed in $[0, 2\pi)$ and α_n is Rayleigh distributed with an exponential power profile

$$\overline{\alpha_n^2} = (1 - e^{-T_s/T_{rms}}) e^{-nT_s/T_{rms}}.$$

with C_L=10, T_{rms}=30ns and T_s=50ns. We use Jakes channel model with maximum Doppler shift of 500 Hz to simulate time-correlated Rayleigh fading α_n.

Fig. 2.8 and **Fig. 2.9** present respectively the BER and MSEE performance of the CFO estimator in frequency-selective fading channels. And we show the MSEE of the channel estimator in **Fig. 2.10**. These performance curves indicate that the BER performance is dominated by the channel estimation error since the MSEE of the CFO estimator is relatively small, especially at high SNRs where the MSEE of our frequency estimate reaches an almost constant floor while the channel estimate's MSEE continues to decrease.
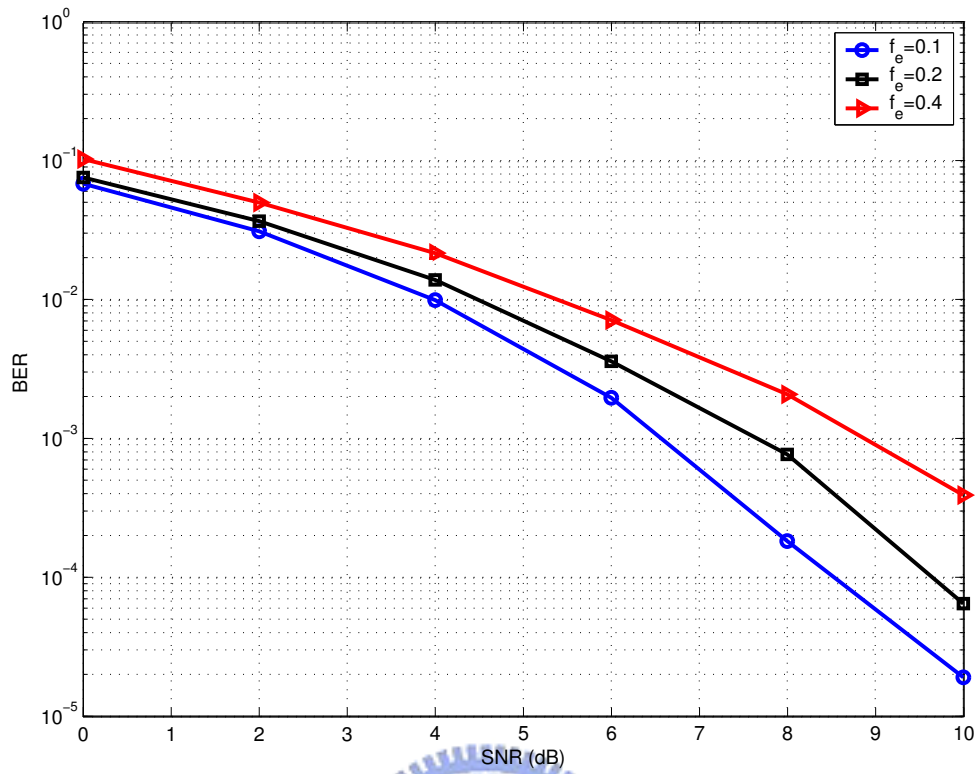
Figure 2.6: BER performance of SISO-OFDM systems using iterative joint FD estimate in AWGN channels with different f_e.
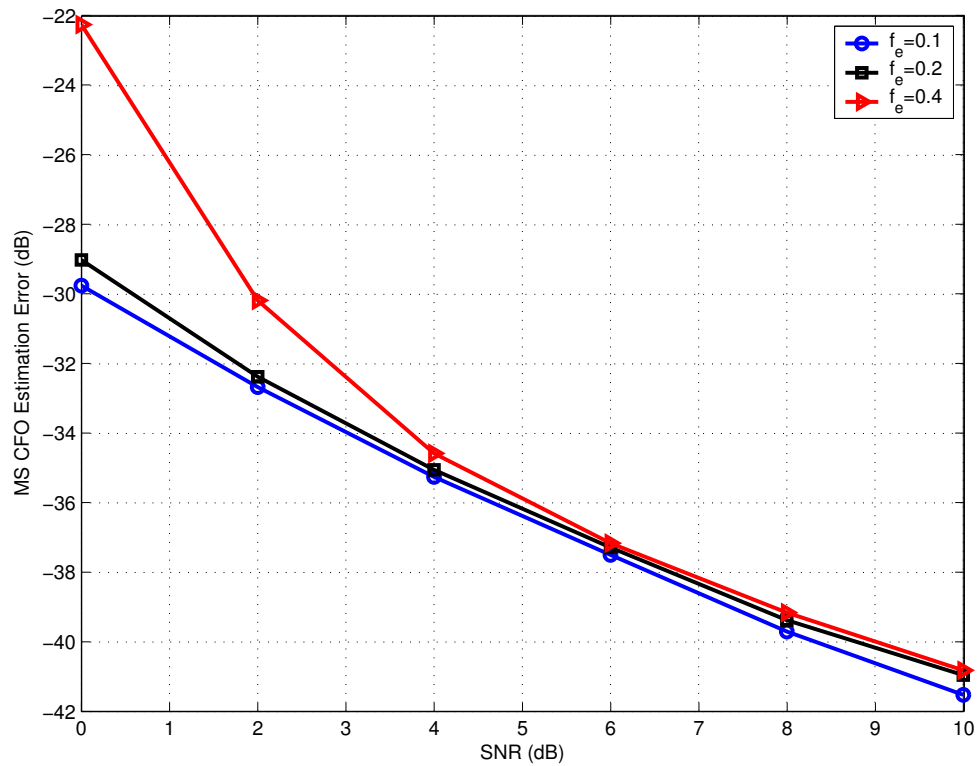
Figure 2.7: MSEE performance of CFO estimates for the joint FD estimate in AWGN channels.
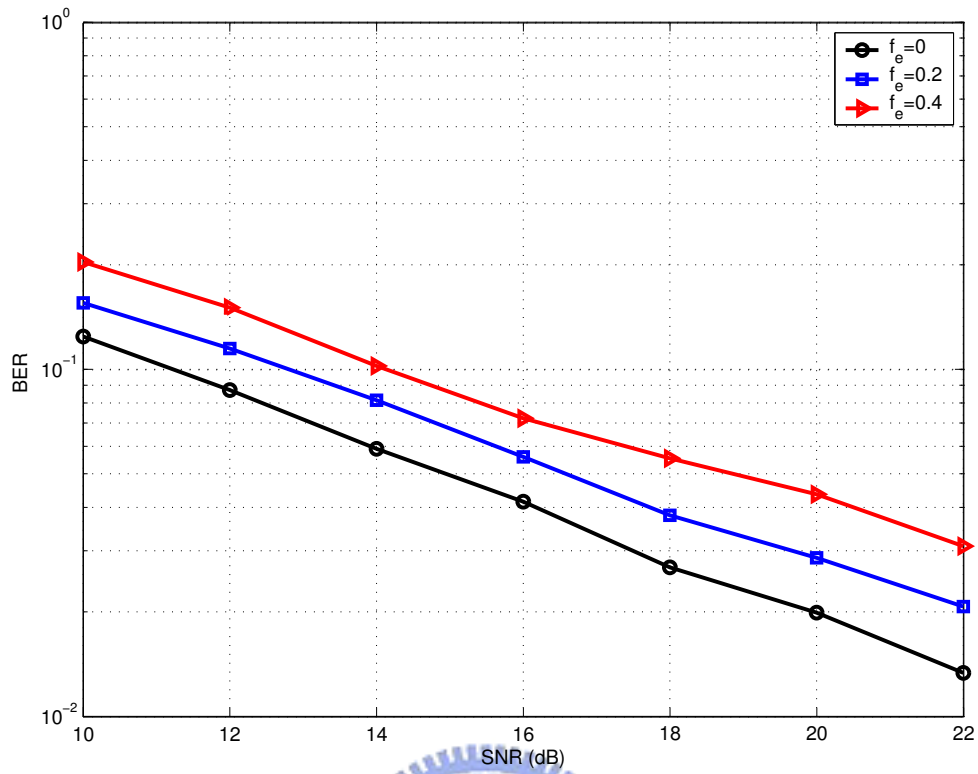
Figure 2.8: BER performance of SISO-OFDM systems using iterative joint FDC estimate in Rayleigh fading channels with different f_e.
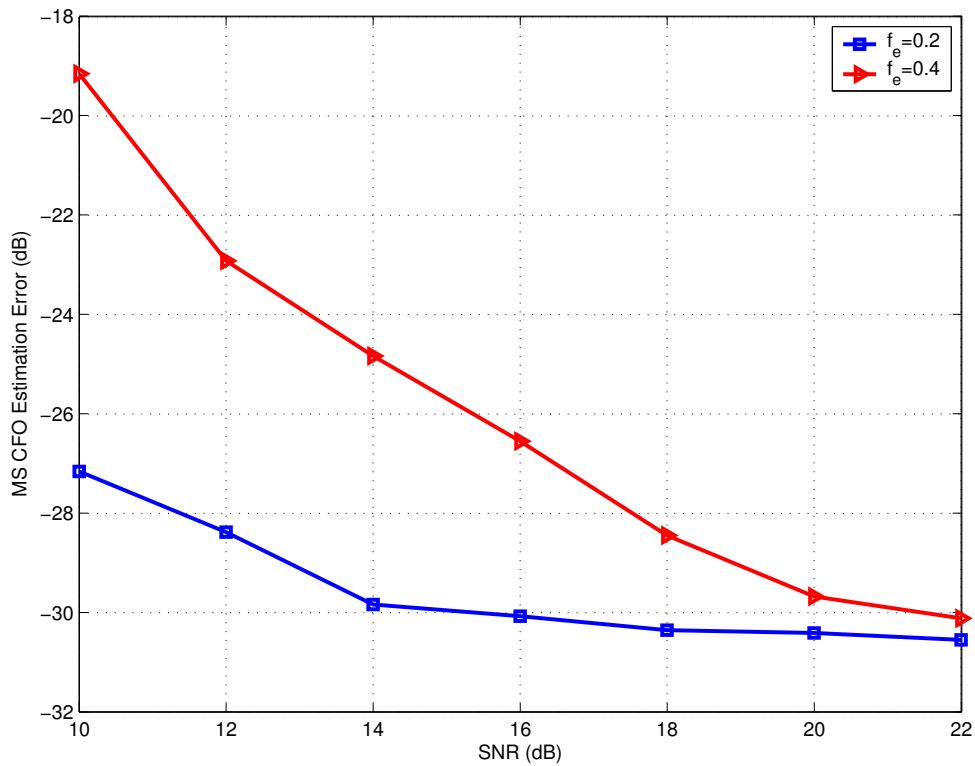
Figure 2.9: MSEE performance of CFO estimates for the joint FDC estimate in Rayleigh fading channels.
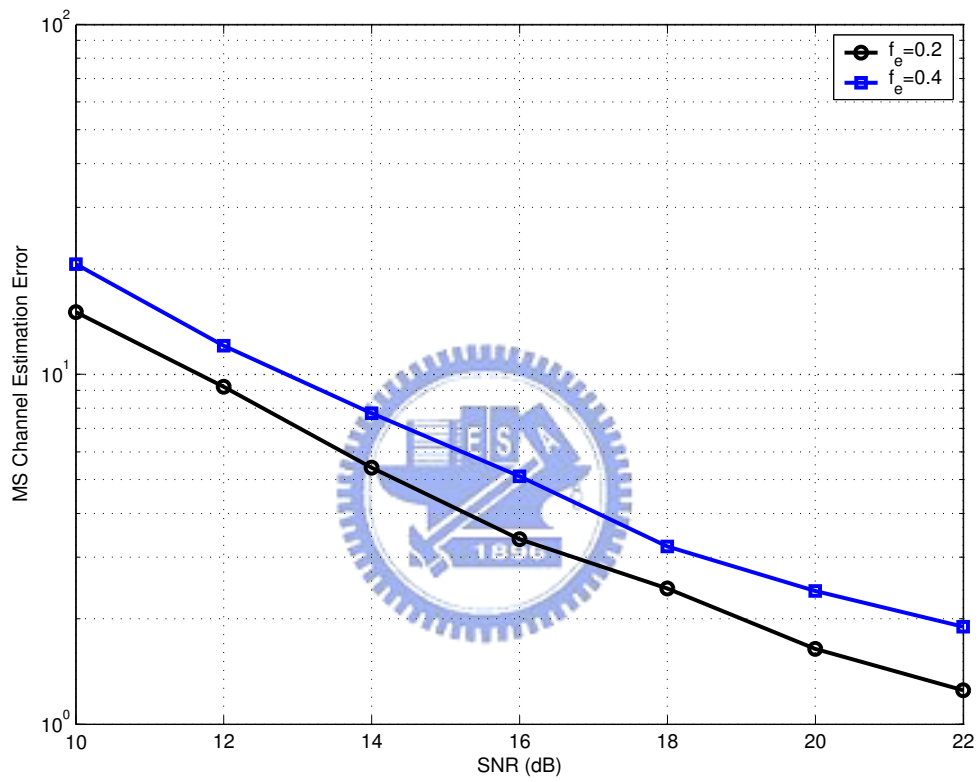
Figure 2.10: MS channel estimation error of the joint FDC estimate in a Rayleigh fading as a function of f_e.

Chapter 3

Further Study on the Detecting SISO-OFDM Signals

This chapter presents two modifications on the algorithm discussed in the previous chapter to enhance the BER (bit error rate) performance. We fist show that, with a proper time-domain windowing in place before the DFT operation, we can reduce the ICI due to CFO. Our second improvement is obtained by using a proper model-based channel estimation method. We demonstrate that improved performance is obtained, especially at high SNRs. Since the complexity of the joint estimator is mostly associated with the Viterbi search, we also show the number of trellis states can be reduced when the normalized absolute CFO is small (≤ 0.2).

3.1   Receiver Window Design

As shown in Chapter 2, conventional OFDM reception [13] makes no use of the signal samples in the guard interval (GI) as they might be corrupted by multipath interference. Only the so-called useful (cyclic prefix-removed) samples are retained and sent to the ensuing discrete Fourier transform (DFT) block for further frequency-domain signal processing. This corresponds to a plain rectangular windowing on the received samples in time domain. Muschalik [14] showed that spectral properties improvement is achieved by allowing excess time in the demodulation window. In many channels, the GI is oversized, i.e., the actual channel-impulse response duration is shorter than the

implemented GI. We refer to that part of the GI which is not affected by echoes from previous OFDM symbols as unconsumed GI. Samples in that region can be exploited to improve performance.

The use of windowing on the time-domain samples before the DFT operation (receiver windowing) reduces the side lobe amplitude but also leads to the loss of orthogonality amongst subcarriers. A window which reduces the side lobes while retains the carrier orthogonality is called a Nyquist window. Muschalik [14] first proposed the use of the raised cosine window to suppress ICI in OFDM systems. Tan and Beaulieu [15] then suggest a new window and claimed that it is superior to the raised cosine window in ICI reduction. These windows need a part of the GI that is not affected by echoes and whose length depends on the channel conditions [18]. As its name suggests, receiver windowing is a receiver-only technique, so it is applicable to systems without requiring a change to the transmitter (which is typically the specified part of a standard).

Other approaches to OFDM transmission with modified window shapes [16] [17], include transmitter modifications to reduce out-of-band power of the transmitter by waveform shaping which is different from the receiver-only approach.

3.1.1 Double-length FFT and square windowing

Since in many cases only a portion of the GI is necessary in order to avoid ISI, the other "variable" part of the GI may be used for Nyquist windowing. We first try to use $2N$ samples in order to maintain the orthogonality.

One way to improve the frequency response of the filter bank is to prolong the rectangular window interval to double its length ($2T_u$) before taking FFT (**Fig. 3.1(a)**). In this case the GI T_g has to be the same length as the usable interval $T_g = T_u$ and has N samples. So now, an FFT of length $2N$ rather than of length N has to be performed, as shown in **Fig. 3.1(b)**. **Fig. 3.1(c)** plots the spectrum of a double length OFDM-symbol. The new filter bank consisting of $2N$ square windowings and the placement of
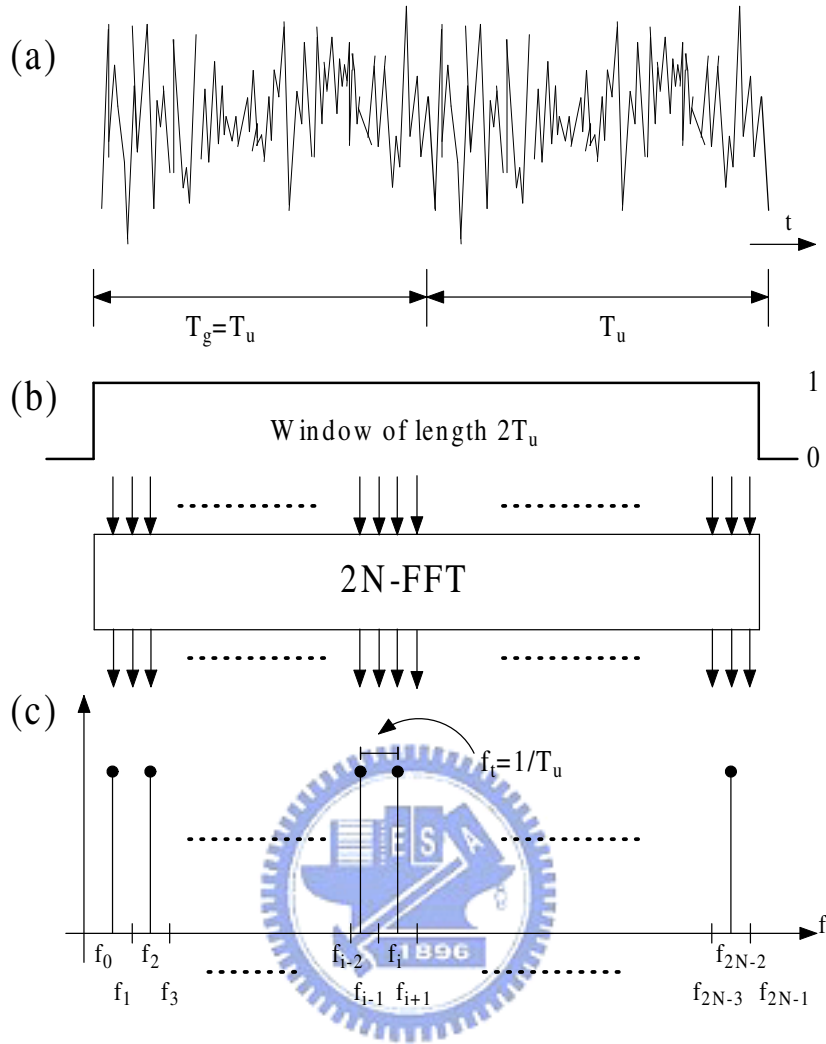
Figure 3.1: Double length of OFDM-symbol(a)time domain, (b)2N rectangular window, (c)frequency domain.

the N carriers are shown in **Fig. 3.2**. We can easily see that there is an additional zero crossing between two carriers. Only the odd or even filters of the filter bank contain the carriers and are used to extract the information. The other so called *ghost* filters contain only disturbances like noise and are not used. Therefore only one half of the $2N$ FFT coefficients need to be calculated to the end. The advantage of having twice as many filters $(2N)$ on the filter bank is that the odd or even filters integrate the same carrier power but only one half of the white noise power of the N-filter case for same maxima value. It results in an improvement on carrier to noise ratio C/N of 3 dB.

21
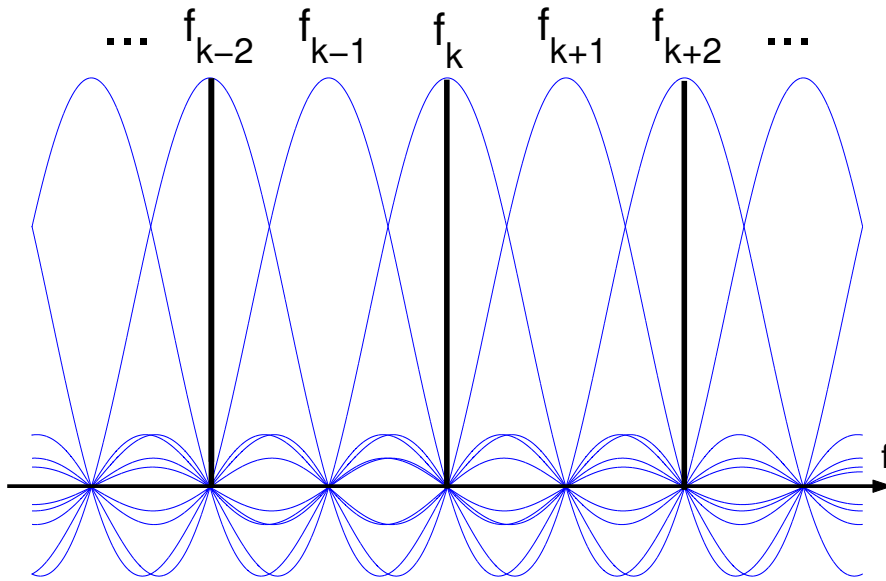
Figure 3.2: Filter bank and the placement of the N carriers

The disturbance power filtered by the "ghost" filters is the gain of this filter bank. The handicap of this kind of windowing is that we need a very long GI ($T_g = T_u$). Therefore the 2N square windowing is under normal conditions unrealizable but, as will be shown in the next subsection, it allows the better understanding of the Nyquist windowing.

3.1.2 Adaptive Nyquist windowing

With GI length between 0 and T_u ,i.e. $T_u \geq T_g \geq 0$, the Nyquist windowing may be implemented to improve the frequency response of the DFT filter. In the case of multipath reception only the "usable GI" T_v is used for the windowing. T_v is supposed to be free of ISI. The windowing is adaptive because T_v depends on channel conditions, hence has **variable** length. **Fig. 3.3** shows the way to implement an adaptive Nyquist windowing.
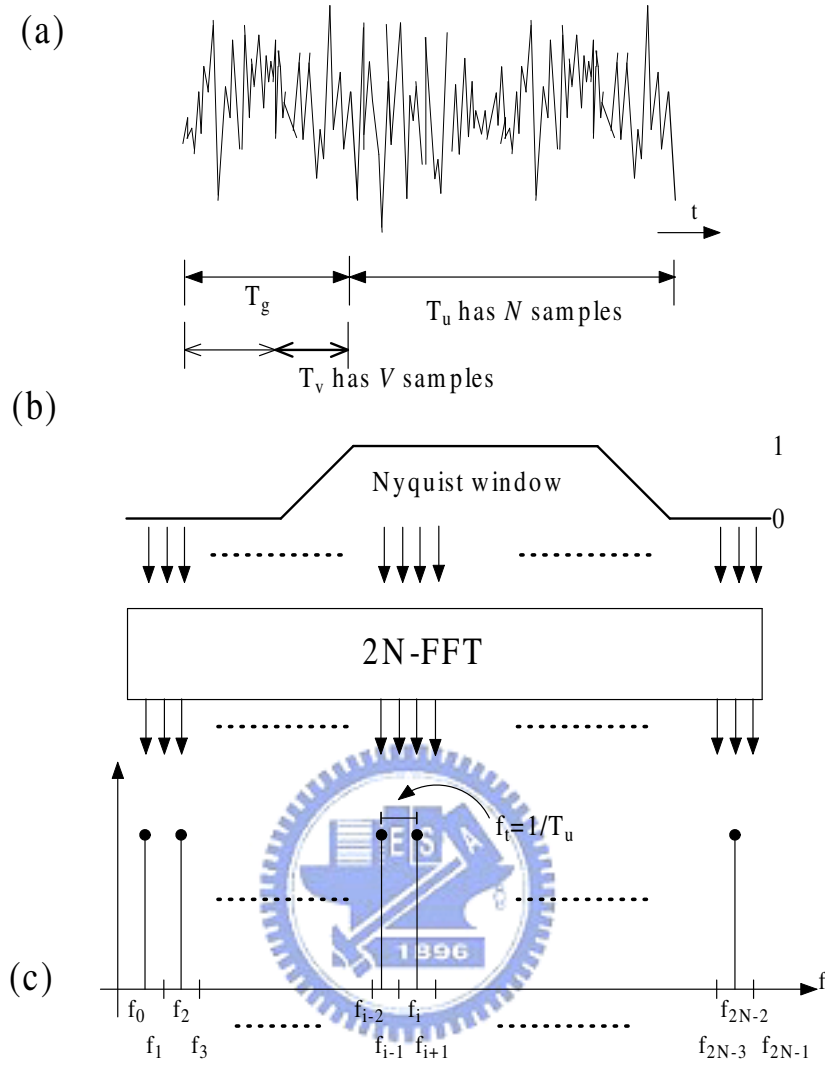
Figure 3.3: Completed OFDM-symbol (a)time domain, (b)Nyquist window, (c)frequency domain.

The usable part of the GI T_v consists of V samples. The V samples of T_v together with the OFDM-symbol T_u (N samples) are symmetrically windowed. The window $w(t)$ has a shape which fulfills the time domain analogy to the Nyquist criterion.

We consider three time-limited pulses. Let $w_r(t)$, $w_{rc}(t)$ and $w_{btrc}(t)$ denote the rectangular pulse, the raised-cosine pulse (in the continuous time domain), and the "better than" raised-cosine (BTRC) pulse (in the time domain) defined as

$$w_r(t) = \begin{cases} \frac{1}{T_u}, & -\frac{T_u}{2} \leq |t| \leq \frac{T_u}{2} \\ 0, & \text{otherwise} \end{cases} \qquad (3.1)$$

23

$$
w_{rc}(t) = \begin{cases} \frac{1}{T_u}, & 0 \le |t| \le \frac{T_u(1-\alpha)}{2} \\ \frac{1}{2T_u}\left\{1 + cos\left[\frac{\pi}{\alpha T_u}\left(|t| - \frac{T_u(1-\alpha)}{2}\right)\right]\right\}, & \frac{T_u(1-\alpha)}{2} \le |t| \le \frac{T_u(1+\alpha)}{2} \\ 0, & \text{otherwise} \end{cases} \quad (3.2)
$$

and

$$
w_{btrc}(t) = \begin{cases} \frac{1}{T_u}, & 0 \le |t| \le \frac{T_u(1-\alpha)}{2} \\ \frac{1}{T_u}e^{\frac{-2ln2}{\alpha T_u}\left[|t| - \frac{T_u(1-\alpha)}{2}\right]}, & \frac{T_u(1-\alpha)}{2} \le |t| \le \frac{T_u}{2} \\ \frac{1}{T_u}\left\{1 - e^{\frac{-2ln2}{\alpha T_u}\left[\frac{T_u(1+\alpha)}{2} - |t|\right]}\right\}, & \frac{T_u}{2} \le |t| \le \frac{T_u(1+\alpha)}{2} \\ 0, & \text{otherwise} \end{cases} \quad (3.3)
$$

with Fourier transforms $W_r(f)$, $W_{rc}(f)$ and $W_{btrc}(f)$, respectively, where α is the roll-off factor, and $0 \le \alpha \le 1$. Here we define $\alpha = T_v/T_u$, which varies depending on the usable part of the GI. **Fig. 3.4** shows the pulse shaping function of raised-cosine pulse and BTRC pulse in time domain with various α. Practical values of α between 0...0.25 may be considered. In our case, we use $\alpha = 0.1$ ($V = 0.1 \times 64 \approx 6$).

If we take $(V + N)$-DFT size after Nyquist windowing, the zero crossings separated by
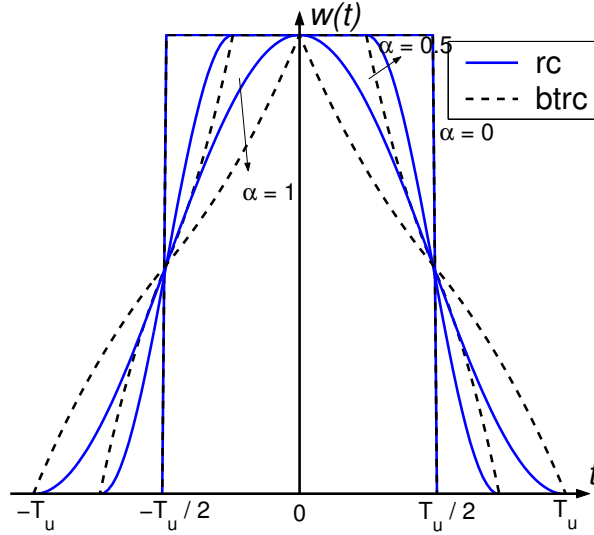
Figure 3.4: The time functions of raised-cosine pulse, and BTRC pulse with different α.

f_t are not the integer times of subcarrier spacing $(1/(T_u + T_v))$. Thus the filter bank has lost its orthogonality. Neither a FFT of the total windowed samples V+N is possible,

because their number is not a power of two. Thus a symmetrical "zero padding" is performed in order to complete a total of 2N samples $s_w[n]$

$$s_w[n] = \begin{cases} 0, & 0 \leq n \leq (N-V)/2 - 1 \\ s[n]w[n] & (N-V)/2 - 1 \leq n \leq 3(N+V)/2 - 1 \\ 0, & 3(N+V)/2 - 1 \leq n \leq 2N - 1 \end{cases} \quad (3.4)$$

where $w[n]$ is the choosing window function after uniform sampling rate $T_u/2N$.

In this way a FFT may still be used instead of the more complex non-power-of-two-DFT and the filter bank orthogonality is restored. The FFT computes the $2N$ coefficients $\mathbf{f}_k$ on the windowed samples $s_w[n]$. **Fig. 3.5** shows the $2N$-FFT filter frequency response $(W_{rc}(f)$ and $W_{btrc}(f))$ depending on the roll-off factor.
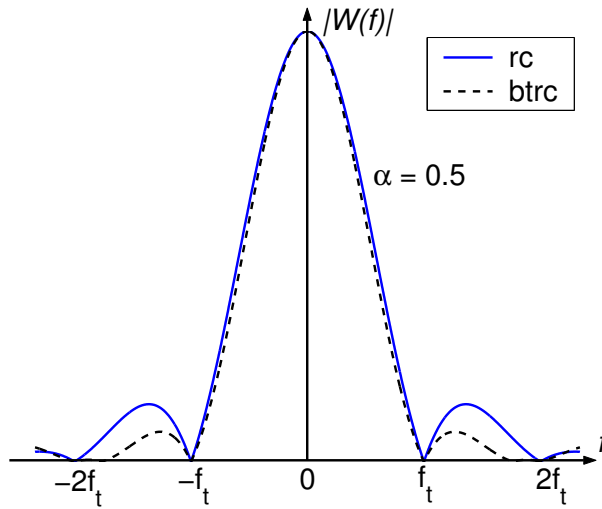
Figure 3.5: Raised cosine window and BTRC window depending of roll-off factor α
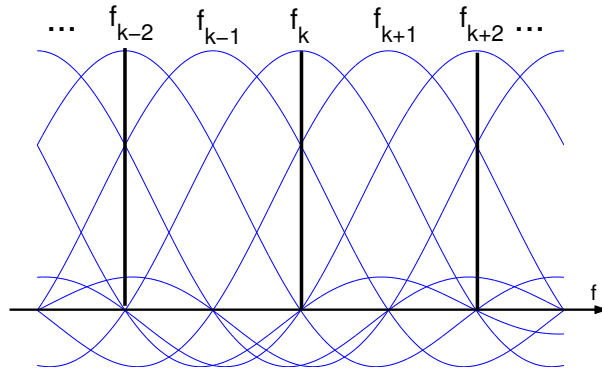
Figure 3.6: DFT-filter bank with Nyquist windowing ($\alpha = 0$)

The filter bank after Nyquist windowing is shown in **Fig. 3.6**. And as the equation shows

$$
\begin{aligned}
y_k &= \sum_{n=0}^{2N-1} s_w[n] e^{-j2\pi nk/(2K)} \\
&= \sum_{n=0}^{2N-1} s_w[n] e^{-j2\pi n(k/2)/K}
\end{aligned}
\tag{3.5}
$$

It is composed of $2N$ filters separated by $f_t/2$. Equation (3.5) reveals that only the odd or even coefficients contain the carrier information, in this case $...y_{k-2}, y_k, y_{k+2}, ...$

26

The other "ghost" coefficients $...y_{k-3}, y_{k-1}, y_{k+1},...$ contain irrelevant information and are not used. We may avoid the computation of these ghost coefficients, decreasing the complexity of the shorted $2N$-FFT near to the complexity of the N-FFT (As a example shown below).

Example:

We assume $N = 4$, and we need a $2N = 8$ FFT in order to implement the Nyquist windowing. A FFT can be graphically represented using butterflies (**Fig. 3.7**) for 8-point, $W_N^k = e^{-j(2\pi/N)k)}$). We can see that one half of the 8-FFT, separated by the dotted line, consists of the odd coefficients and the other half consists of the even coefficients. Therefore it is not necessary to compute one half of the coefficients of the 2N-FFT until the end. We only need to compute the first stage of the 2N-FFT before computing the remaining N-FFT.
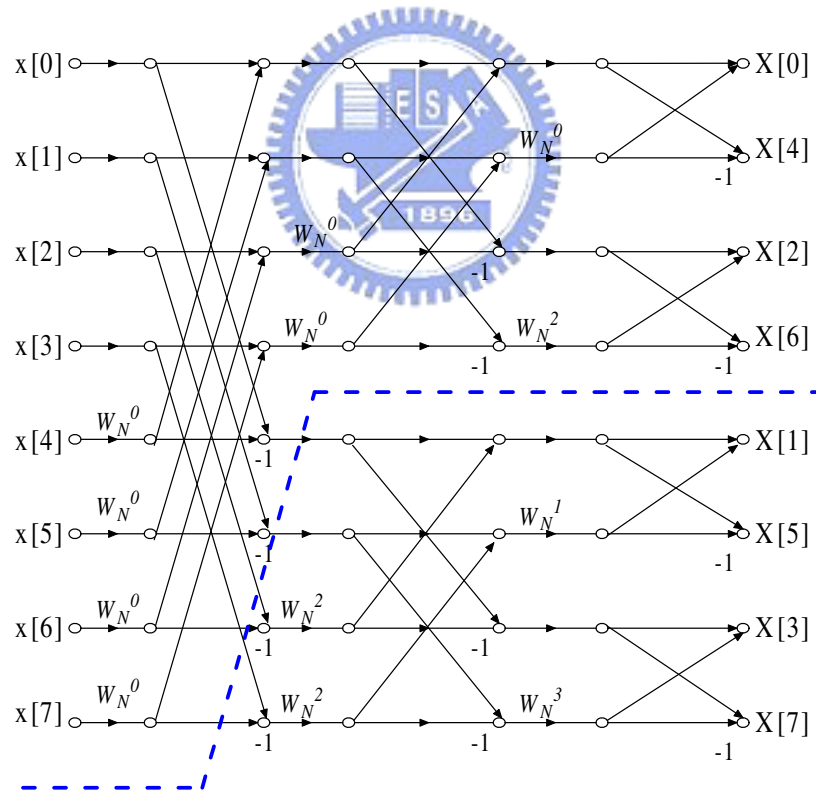
Figure 3.7: Graphical representation of a 8-FFT

3.1.2.1 "Folding" method

If we observe (3.5) further, it can be rewrite as follows :

$$
\begin{aligned}
y_k &= \sum_{n=0}^{N-1} s_w[n]e^{-j2\pi n(k/2)/K} + \sum_{n=N}^{2N-1} s_w[n]e^{-j2\pi n(k/2)/K} & (3.6)\\
&= \sum_{n=0}^{N-1} (s_w[n] + s_w[n+N])e^{-j2\pi n(k/2)/K} \qquad \text{if } k \in \text{even numbers} & (3.7)
\end{aligned}
$$

After multiplying the received sequence in an OFDM symbol by the window function, the last V samples in GI, which are covered by the window function, are added to the last V samples in the symbol. Then, GI is excluded and the remaining N samples are fed into the FFT module. Let $k = 2k'$ we can rewrite (3.7) as

$$
y_{k'} = \sum_{n=0}^{N-1} \tilde{s}[n]e^{-j2\pi nk'/K} \qquad , k' = 0, 1, ..., N-1 \qquad (3.8)
$$

where $\tilde{s}[n] = s_w[n] + s_w[n+N]$ for $n = 0, 1, ..., N-1$. $\tilde{s}[n]$ is referred to as the "folding window signal".

In summary, as a shortened $2N$-FFT avoids the computation of ghost coefficients, we find that $2N$-FFT can be replaced by N-FFT with proper processing before the FFT operation as shown in **Fig. 3.8** [20] [21].
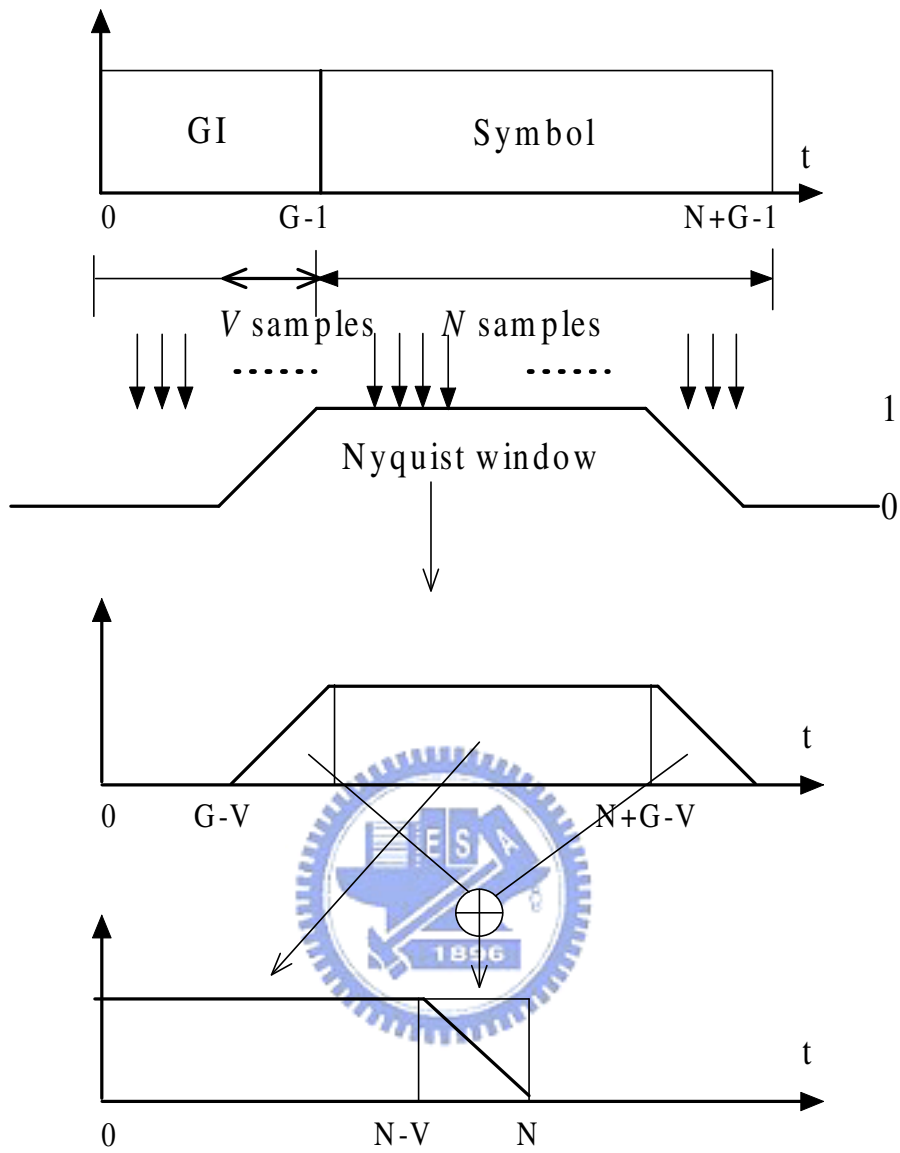
Figure 3.8: Folding of the receiver window.

3.1.3 Effect of windowing on ICI and noise Power

3.1.3.1 ICI Analysis

After a width-$2N$ windowing, the received signal part with a normalized CFO f_e is

$$
\begin{aligned}
y_k &= \frac{1}{N} \sum_{n=0}^{2N-1} s[n]w[n]e^{-j2\pi nk/(2N)} \\
&= \sum_{m=0}^{N} a_m \left\{ \frac{1}{K} \sum_{n=0}^{2N-1} w[n]e^{-j2\pi n(k/2-m)/N}e^{j2\pi f_e n/N} \right\} \\
&= \sum_{m=0}^{N} a_m \left\{ \frac{1}{K} \sum_{n=0}^{N-1} (w[n]+w[n+N])e^{-j2\pi n(k/2-m)/N}e^{j2\pi f_e n/N} \right\} \quad \text{if } k \in \text{even numbers} \\
&= \sum_{m=0}^{N} a_m \left\{ \frac{1}{K} \sum_{n=0}^{N-1} w_N[n]e^{-j2\pi n(k/2-m)/N}e^{j2\pi f_e n/N} \right\} \quad \text{if } k \in \text{even numbers} \quad (3.9)
\end{aligned}
$$

where $w_N[n] = w[n] + w[n+N] \qquad n = 0,1,...,N-1$

After even sampling, i.e. letting $k = 2k'$, we have

$$
y_{k'} = a_{k'}W_0^{f_e} + \underbrace{\sum_{m\neq k'} a_m W_{k'-m}^{f_e}}_{\text{ICI}} \quad \text{for } 0 \leq k' \leq N-1 \qquad (3.10)
$$

where $W_k^{f_e}$ is the N-FFT of $w_N(n)$ with f_e. Hence, the power of the desired signal is

$$
\sigma_{k'} = |a_{k'}|^2 |W_0^{f_e}|^2 \qquad (3.11)
$$

and the corresponding ICI power is

$$
\sigma_{\text{ICI}}^{k'} = \sum_{m=0,m\neq k'}^{N-1} \sum_{n=0,n\neq k'}^{N-1} a_m a_n^* W_{m-k'}^{f_e} W_{n-k'}^{f_e} \qquad (3.12)
$$

The ICI power depends not only on the desired symbol location, k', and the transmitted symbol sequence but also on the pulse-shaping function and the number of subcarriers. Taking average over different independent data sequences on (3.12) gives the average ICI power

$$
\overline{\sigma_{\text{ICI}}^{k'}} = \sum_{m=0,m\neq k'}^{N-1} |W_{m-k'}^{f_e}|^2 \qquad (3.13)
$$

30

For the Nyquist window pulse, one has (see **Fig. 3.5**)

$$|W_{r,m-k'}^{f_e}| \geq |W_{rc,m-k'}^{f_e}| \qquad (3.14)$$

$$|W_{r,m-k'}^{f_e}| \geq |W_{btrc,m-k'}^{f_e}| \qquad (3.15)$$

Therefore, a rectangular pulse-shaped OFDM system always has larger ICI power than that associated with a raised-cosine pulse-shaped OFDM system or a BTRC pulse-shaped OFDM system. **Fig. 3.9** compares the ICI power when $\alpha = 0.1$ for the rectangular pulse, raised-cosine pulse and BTRC pulse. **Fig. 3.10** shows a similar comparison for the case of $\alpha = 1$. Noteworthy, for the same value of α, the BTRC pulse outperforms the raised-cosine pulse despite the fact that the tails of $W_{btrc}(f)$ and $W_{rc}(f)$ decay as f^{-2} and f^{-3} , respectively. This is because the sum (3.13) is completely dominated by the closest two terms.

Comparing **Fig. 3.9** and **Fig. 3.10**, we find that increasing α leads to large ICI power reduction. This is expected since increasing α corresponds to reducing the side-lobes in the spectrum.

We now examine the impact of the baseband pulse used in terms of the average signal power to average ICI power ratio (SIR). Averaging (3.11) over all possible transmitted symbols and combining with (3.12) yields

$$\text{SIR} = \frac{|W_0^{f_e}|^2}{\sum_{m=0,m\neq k'}^{N-1} |W_{m-k'}^{f_e}|^2} \qquad (3.16)$$

Fig. 3.11 compares the SIR for different pulse-shaping functions in a 64-subcarrier OFDM system plotted as functions of the normalized frequency offset, f_e. Observe that the BTRC pulse outperforms the raised-cosine pulse. For example, assume that it is desired to track CFO range less than 0.25. When employing the BTRC pulse, the SIR can maintain at least 7.1656 dB. In contrast, the SIR_{min} is only 6.8966 dB when one uses the raised-cosine pulse. The difference of SIR_{min} between two pulses will become wider as α increases.
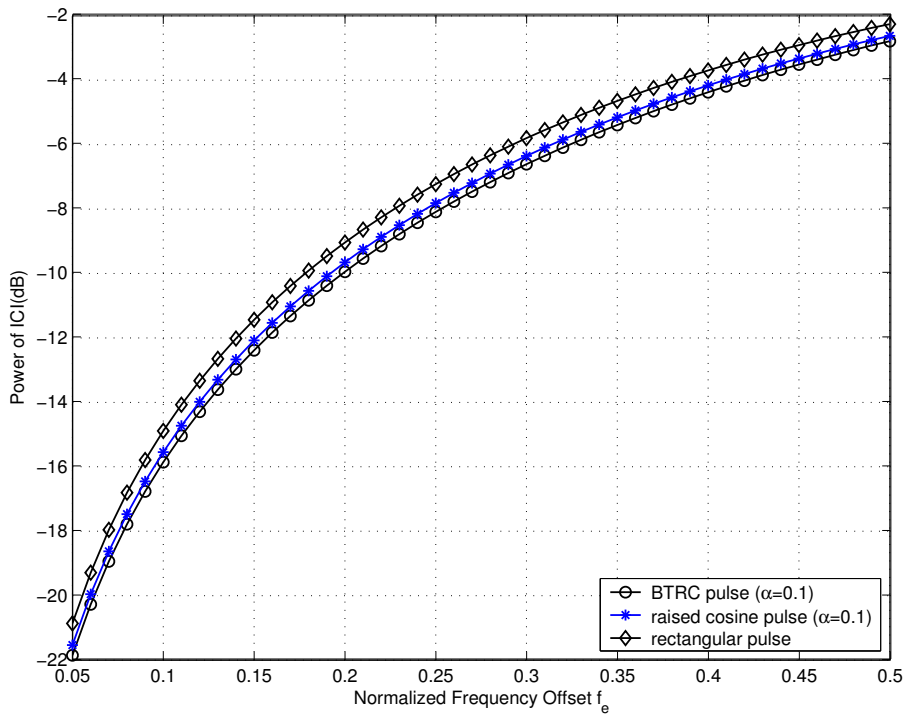
Figure 3.9: Comparison of ICI power for different baseband pulse-shaping functions ($\alpha = 0.1$) in a 64-subcarrier OFDM system.
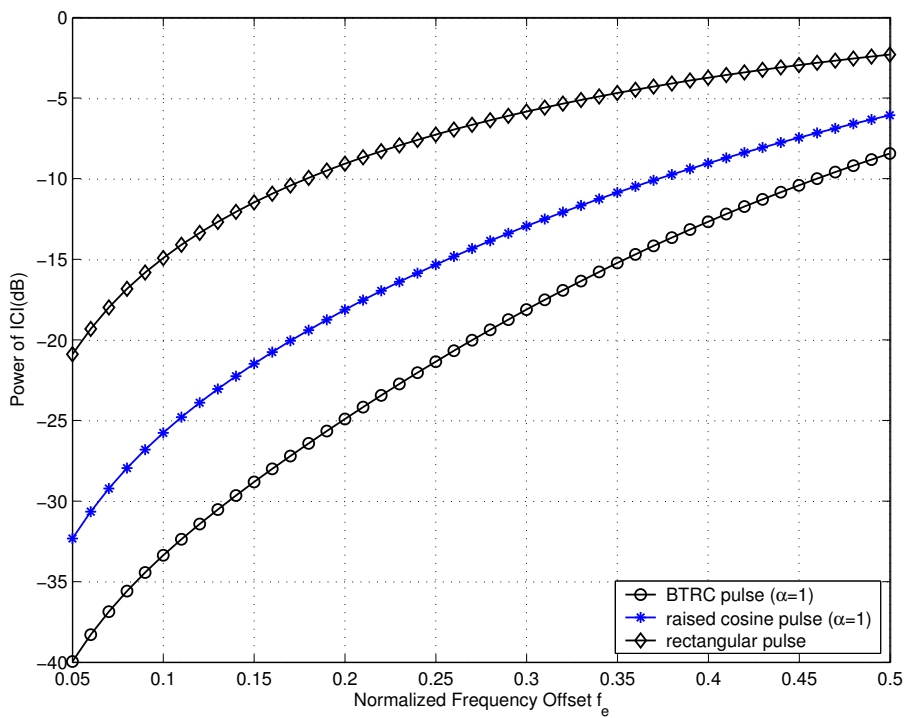
Figure 3.10: ICI power associated with different base pulse-shaping functions ($\alpha = 1$) in a 64-subcarrier OFDM system.

32
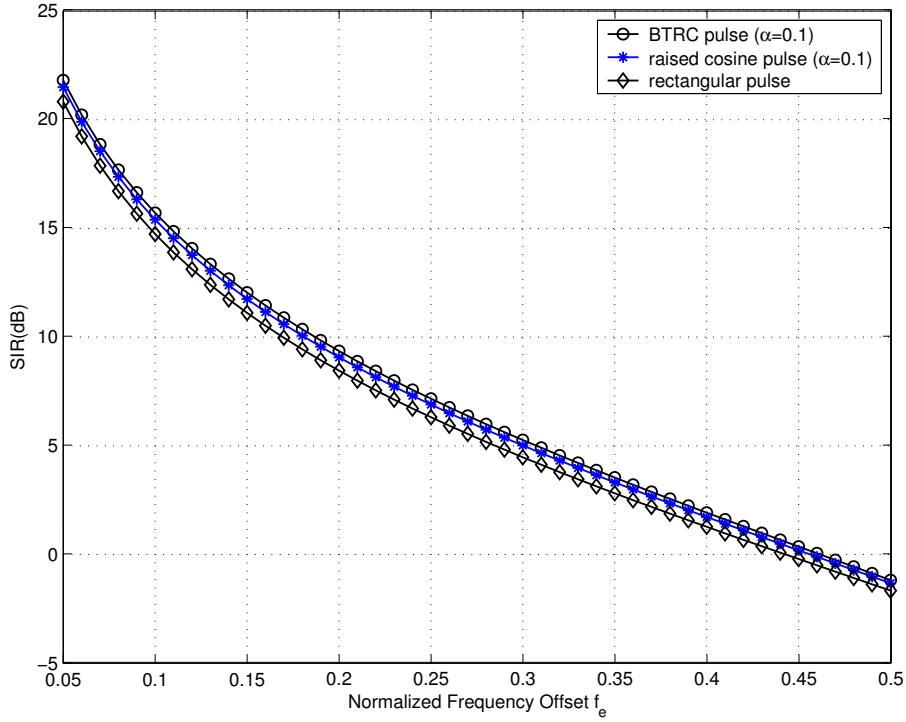
Figure 3.11: SIR for different baseband pulse-shaping functions ($\alpha = 0.1$) in a 64-subcarrier OFDM system.

3.1.3.2 Noise power analysis

The noise component of the received frequency domain samples at subcarrier k can be written as

$$n_k = \sum_{n=0}^{2N-1} n'[n]w[n]e^{-j2\pi nk/2N} \tag{3.17}$$

where $n'[n]$ is independent complex Gaussian random noise value before windowing at time n and has zero mean and variance $\sigma_{n'}^2 = N_0$. The power of the noise on sub-carrier k is

$$
\begin{aligned}
\sigma_n^2 &= E[n_k n_k^*] \\
&= \sum_{m=0}^{2N-1} \sum_{n=0}^{2N-1} E[\, n'[m]n'^*[n] \,]\, w[m]w^*[n]\, e^{-j2\pi nk/2N} e^{j2\pi nk/2N} \\
&= \sigma_{n'}^2 \sum_{m=0}^{2N-1} |w[m]|^2 \tag{3.18}
\end{aligned}
$$

Since $\sum_{m=0}^{2N-1} |w[m]|^2 = \frac{1}{2N} \sum_{k=0}^{2N-1} |W_k|^2$ (by Parseval's Theorem), one can easily conclude that with proper Nyquist window, it will not only reduce the ICI power but also the noise power.

3.1.4 Complexity issue

The complexity of an N-FFT may be measured by the number of complex multiplications performed M. The sums (additions) does not represent a major increase in complexity since they may be performed very easy. For a radix-2 algorithm [8],

$$M = \frac{N}{2} log_2(N) \tag{3.19}$$

$2N$-**FFT** : As shown in **Fig. 3.7**. Since the first stage of a FFT normally consists of trivial multiplications (1 ,- 1, j, - j), the complexity of the N-FFT (M multiplications, N sums) is nearly the same that the complexity of the "shorted" $2N$-FFT (M non-trivial multiplications, $2N$ sums).

"Folding" method: After the variable length of CP multiplied by the V samples of window and are added to the last V samples in the symbol, the remaining V samples are fed into the N-point FFT module whose complexity is almost the same as a $2N$-point FFT. We thus conclude that the receiver windowing is a computationally reasonable operation.

3.2 Reducing the Number of Trellis States

The complexity of the joint estimation algorithm is mostly associated with the Viterbi search. The state number is M^{2L} states where M is the modulation order and $2L$ is the considering "CFO channel length" (Section 2.1.2). It will cause time-consuming search if the modulation order is large; The complexity grows exponentially with the number of transmit antennas (M^{2L*M_T} states) if we extend the algorithm to MIOM OFDM systems (Chapter 4).

Based on above discussion, it is desirable to construct a detection method that reduces

the complexity of the Viterbi algorithm by "shortening" the memory of the "CFO channel".

Since the BTRC window has best property to lower the ICI effect among rectangular window and raised-cosine window, it becomes our favorable candidate.

Consider a residual CFO less than 20% of the subcarrier spacing, we would like to direct truncation of the nonsignificant side channel response. Here, we judge tap $W_k^{f_e}$ to be non-significant if $|W_k^{f_e}|^2 / \sum_k |W_k^{f_e}|^2 < 0.01$. As shown in **Fig. 3.12** for BTRC window, there has only three taps after truncation.

Further, we use delayed decision-feedback sequence estimation (DDFSE) algorithm[22], and force the number of considering channel taps down to 2. The algorithm combines structures of the reduced-state Viterbi algorithm and decision-feedback detector and provides a tradeoff between complexity and performance.
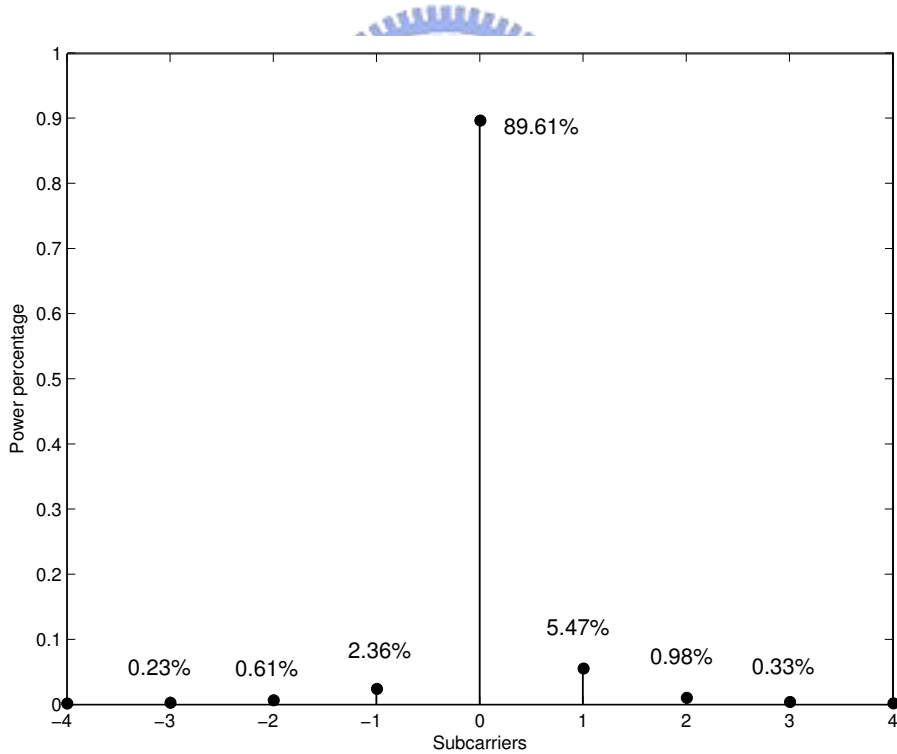
Figure 3.12: Power percentage distribution of BTRC in frequency domain for each subcarrier at CFO = 0.2.

3.2.1 Complexity issue

Since the total levels of the "reduced-state" approach are the same as the "full-state" approach in Viterbi search, we consider the complexity across two levels only. For the "full-state" approach, one has to compute M branches for every node with $2L+1$ complex multiplications performed at each branch. The total number of nodes is equal to M^{2L}. So, $M^{2L} \times M(2L+1) = (2L+1)M^{2L+1}$ complex multiplications and M^{2L} comparisons are needed to enter the next level (here $L = 2$ is used). On the other hand, the "reduced-state" approach used here needs $M \times M \times 3 = 3M^2$ complex multiplications and M comparisons only.

3.3 Channel Estimation

Since in our CFO estimator for frequency-selective Channels (Section 2.2), the initial channel estimate comes directly from the previous OFDM symbol, the performance of the present symbol is dependent on that of the previous symbol and error propagation is likely to occur. We now examine the effectiveness of the novel model-based estimation method [24] for estimating channels.

3.3.1 Jakes model

The Jakes fading model is a deterministic method for simulating time-correlated Rayleigh fading waveforms [23] and is widely used today. The model assumes that N equal-strength rays arrive at a moving receiver with uniformly distributed arrival angles α_n, such that ray n experiences a Doppler shift $\omega_n = \omega_M cos(\alpha_n)$, where $\omega_M = 2\pi f_c v/c$ is the maximum Doppler shift, v is the vehicle speed, f_c is the carrier frequency, and c is the speed of light. Using $\alpha_n = 2\pi n/N$ (see **Fig. 3.13**), there is quadrantal symmetry in the magnitude of the Doppler shift, except for angles 0 and π. As a result, the fading waveform can be modelled with $N_0 + 1$ complex oscillators, where $N_0 = (N/2 - 1)/2$.
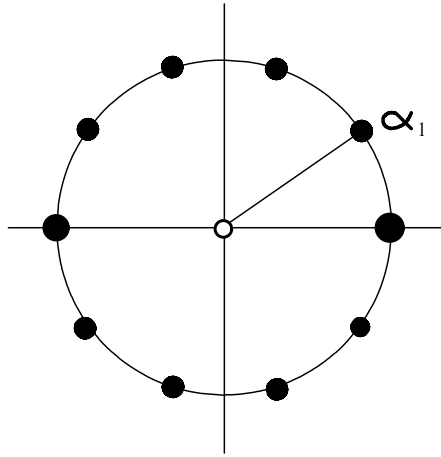
Figure 3.13: Ray arrival angles in the Jakes model ($N = 10$).

This gives

$$
\begin{aligned}
T(t) &= K\{\frac{1}{\sqrt{2}}[\cos(\alpha) + j\sin(\alpha)]\cos(\omega_M t + \theta_0) \\
&+ \sum_{n=1}^{N_0}[\cos(\beta_n) + j\sin(\beta_n)]\cos(\omega_n t + \theta_n)\}
\end{aligned}
\tag{3.20}
$$

K is a normalization constant, α (not the same as α_n.) and β_n are phases, and θ_n, are initial phases usually set to zero. Setting $\alpha = 0$ and $\alpha_n = \pi n/(N_0 + 1)$ gives zero cross-correlation between the real and imaginary parts of T(t).

Jakes model is a very popular channel model for mobile multipath channels that takes into account the Doppler effect and is based on the assumptions that the receiver is moving at speed v while the arrival angles of multipath components are uniformly distributed. The time correlation of the channel is given by

$$
R(\Delta t) = J_0(2\pi \cdot \Delta t \cdot f_d) \tag{3.21}
$$

where Doppler frequency $f_d = v \cdot f_c/c$. $J_0(x)$ is the zero-*th* order Bessel function of the first kind.

Real part of channel : $ch_v = 108$ km/hr
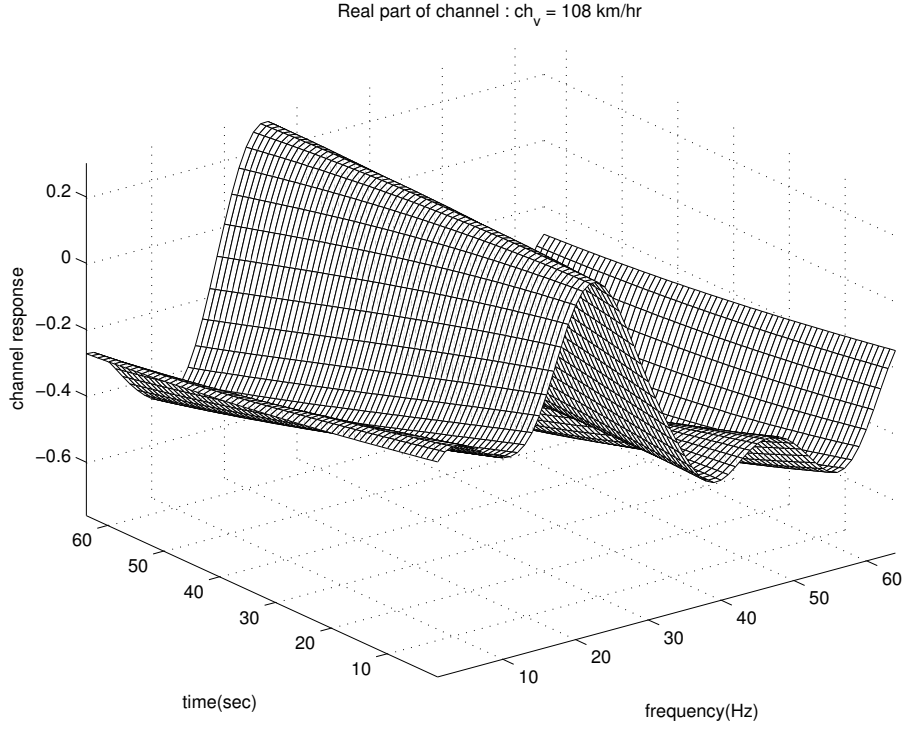
Figure 3.14: Real part of a Jakes fading process.

3.3.2 Model-based channel estimate

(2.14) of Section 2.2 gives an LS channel estimate which can be rewritten as

$$\hat{H}_{ls}(m,n) = \frac{R(m,n)}{X(m,n)} = H(m,n) + \frac{Noise(m,n) + ICI(m,n)}{X(m,n)}, \qquad (3.22)$$

where $H(m,n)$, $X(m,n)$ and $R(m,n)$ denote respectively the channel response, transmitted signal and received samples at the mth subcarrier during the nth symbol interval. The channel responses $H(m,n)$ can be viewed as a sampled version of the two-dimension (2D) continuous complex fading process $H(f,t)$ (**Fig. 3.14**). We choose a operating region in the time-frequency plane and model the sampled fading process $H(m,n)$ in this region by the quadrature surface

$$H_{model}(x,y) = ax^2 + bxy + cy^2 + dx + ey + f \qquad (3.23)$$

38

where the coefficients (a, b, c, d, e, f) are chosen such that

$$\sum_{(m,n)} \left| \hat{H}_{ls}(m,n) - H_{model}(m,n) \right|^2 \qquad (3.24)$$

is minimized. Rewriting (3.24) in a more compact form

$$\sum_{(m,n)} \left| \hat{H}_{ls}(m,n) - \mathbf{q}_{m,n}^T \mathbf{c} \right|^2 \qquad (3.25)$$

where $c^H = (a, b, c, d, e, f)$ is the coefficient vector and $q_{m,n}^T = (m^2, mn, n^2, m, n, 1)$ is the data location vector, we can show

$$\hat{\mathbf{c}} = \arg\min_{c} \left\| \hat{\mathbf{H}}_{ls} - \mathbf{Q}\mathbf{c} \right\|^2 \qquad (3.26)$$

where $\hat{\mathbf{H}}_{ls} = (\hat{H}_{ls}(0,0), \hat{H}_{ls}(0,1), ..., \hat{H}_{ls}(L_f - 1, L_t - 1))^T$ and

$$\mathbf{Q} = \begin{pmatrix} \mathbf{q}_{0,0}^T \\ \mathbf{q}_{0,1}^T \\ \vdots \\ \mathbf{q}_{L_f-1,L_t-1}^T \end{pmatrix} = \begin{pmatrix} 0 & 0 & 0 & \cdots & 1 \\ 0 & 0 & 1 & \cdots & 1 \\ \vdots & \vdots & \vdots & \ddots & \vdots \\ (L_f-1)^2 & (L_f-1)(L_t-1) & (L_t-1)^2 & \cdots & 1 \end{pmatrix}$$

L_f and L_t are the block length of freq and time respectively. Note that from (3.23) $\mathbf{Q}\hat{\mathbf{c}}$ represents the new estimate of the channel impulse response. By solving (3.26), the coefficients of the regression polynomial is

$$\hat{\mathbf{c}} = (\mathbf{Q}^T \mathbf{Q})^{-1} \mathbf{Q}^T \hat{\mathbf{H}}_{ls}, \qquad (3.27)$$

and we obtain the new estimates

$$\hat{\mathbf{H}}_{\text{model}}(m,n) = \mathbf{q}_{m,n}^T \hat{\mathbf{c}}. \qquad (3.28)$$

$$\hat{\mathbf{H}}_{\text{model}} = \mathbf{Q}\hat{\mathbf{c}} = \mathbf{Q}(\mathbf{Q}^T \mathbf{Q})^{-1} \mathbf{Q}^T \hat{\mathbf{H}}_{ls} = \mathbf{V}\hat{\mathbf{H}}_{ls}, \qquad (3.29)$$

where

$$\mathbf{V} = \mathbf{Q}(\mathbf{Q}^T \mathbf{Q})^{-1} \mathbf{Q}^T. \qquad (3.30)$$

Fig. 3.15 indicates the fitting processing of one-dimension (1-D). We can infer that if the SNR is high enough, the regression may improve the channel estimation.

39
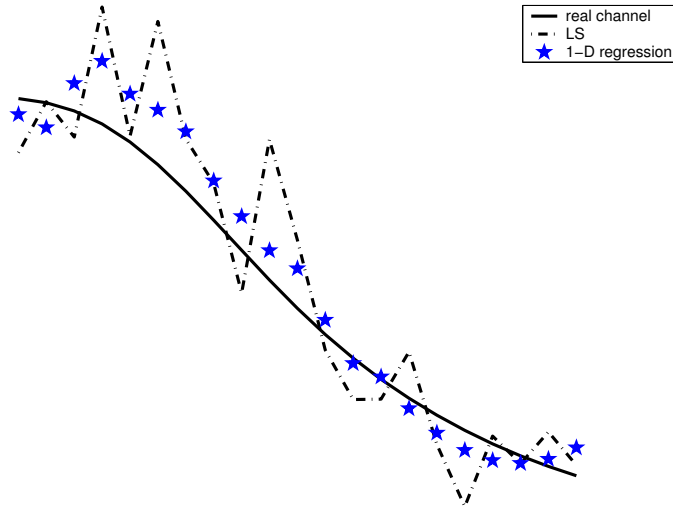
Figure 3.15: Regression of LS channel under SNR=12dB.

3.3.3 2D model-based channel estimate with transform-domain processing (2-D+TDP)

A channel estimation based on transform-domain processing was proposed in [25]. This method employs lowpass filtering in the transform domain so that ICI and additive AWGN components in the received pilots are significantly reduced.

Although we can not get the information from a side band, we can still use the regression model of the previous subsection to suppress the effects of ICI and AWGN in the transform-domain. **Fig. 3.16** is a block diagram that represents an improved channel estimator, concatenating the transform-domain processing algorithm with the 2D model-based channel estimator.
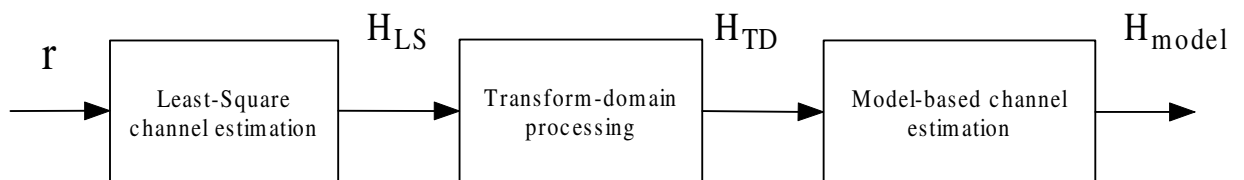
Figure 3.16: A complete channel estimation process.

3.3.4 Complexity issue

Suppose there are N_u modulated subcarriers in the transmitted waveform, an LS channel estimate needs N_u complex divisions or $5N_p$ multiplications per OFDM symbol. It is thus preferred to use (3.29) from a complexity point of view. The resulting computational algorithm is

$$\hat{\mathbf{c}} = \mathbf{P}\hat{\mathbf{H}}_{ls}, \tag{3.31}$$

$$\hat{\mathbf{H}}_{\text{model}}(m, n) = \mathbf{q}_{m,n}^T \hat{\mathbf{c}}. \tag{3.32}$$

where $\mathbf{P} = (\mathbf{Q}^T\mathbf{Q})^{-1}\mathbf{Q}^T$ is a constant matrix with dimension $length(\mathbf{c}) \times (L_f \cdot L_t)$. To obtain $\hat{\mathbf{c}}$ we need $2\, length(\mathbf{c})L_f L_t$ real multiplications since $\mathbf{P}$ is real. Calculating each channel response at the data tone using (3.32) needs $2\, L_f L_t$ real multiplications. Since there are N_u modulated subcarriers, we totally need $2N_u(length(\mathbf{c}) + 1)L_f L_t$ real multiplications for an OFDM symbol.

The transform-domain based channel estimate uses two FFTs (both of size is N_u) to estimate the channel response. For a radix-2 algorithm, the total number complex multiplications required is about $N_u log_2(N_u)$ and need $2N_u(length(\mathbf{c}) + 1)L_f$ real multiplications for regression in the transform-domain. On the other hand, the proposed 2-D regression model needs $L_f N_u$ memory to store those symbols information. The 1D channel estimate does not need any extra memory to save symbol information.

3.4 Numerical Experiments

In previous sections, we have presented several methods either to enhance performance or to reduce complexity of a joint estimation-detection process. This section gives some numerical experimental results on these improvements. We first compare the BER performance of the conventional Nyquist window (raised-cosine window) with that of rectangular windowing in AWGN channels (**Fig. 3.17**). In **Fig. 3.18**, we then proceed to examine the performance in Rayleigh fading channels. We find that the BTRC

41

window offers a superior performance for OFDM systems with nonzero CFO. One observes that the BER performance is almost undistinguishable for different windowing at small SNRs. This is because BER performance is dominated by AWGN at small SNRs and is determined by the ICI at high SNRs. The almost-flat curve represents the performance of a receiver that does not update channel estimate, using the pilot-assisted estimate for detecting the data payload. It obvious that channel updates are needed in a time-varying channel to have reliable decisions. **Fig. 3.19** proves the importance of the channel estimation method used and indicates that the regression model-based algorithm does offer reliable channel estimates. Finally, **Fig. 3.20** reveals that the reduced-state algorithm is effective for it incurs less than 0.6 dB BER performance loss within the range of interest.

Figure 3.17: BER performance of SISO-OFDM systems using iterative joint FD estimate with different windowing in AWGN channels.

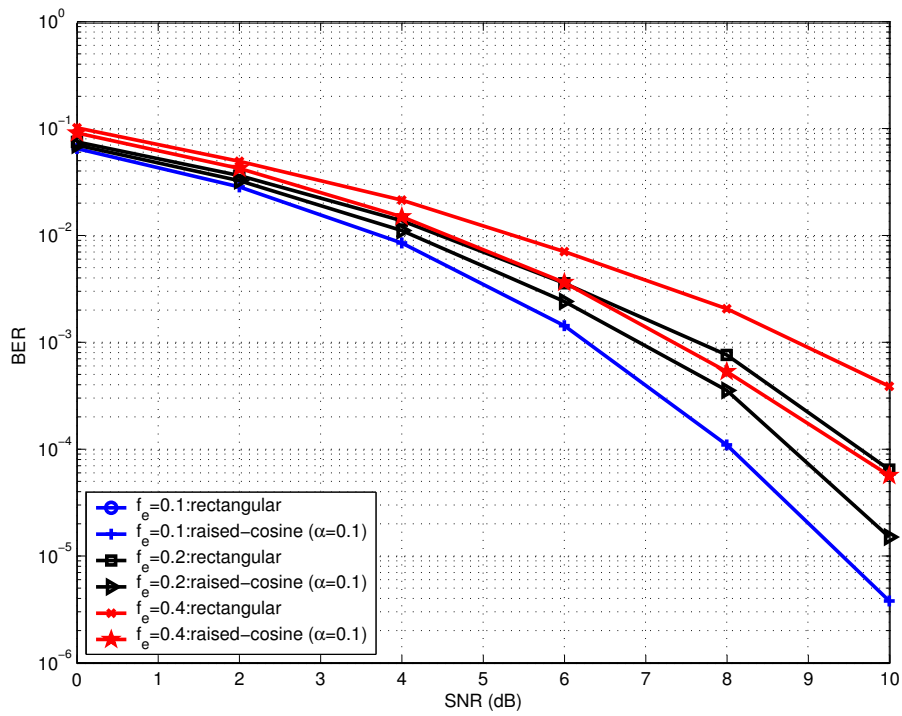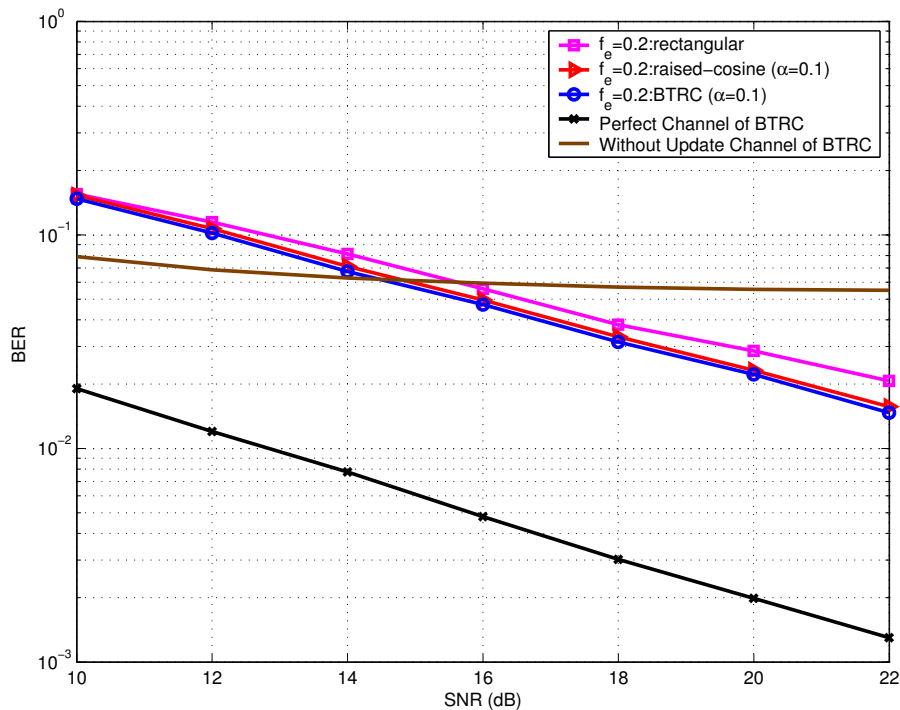Figure 3.18: BER performance of SISO-OFDM systems using iterative joint FDC estimate with different windowing in Rayleigh fading channels.
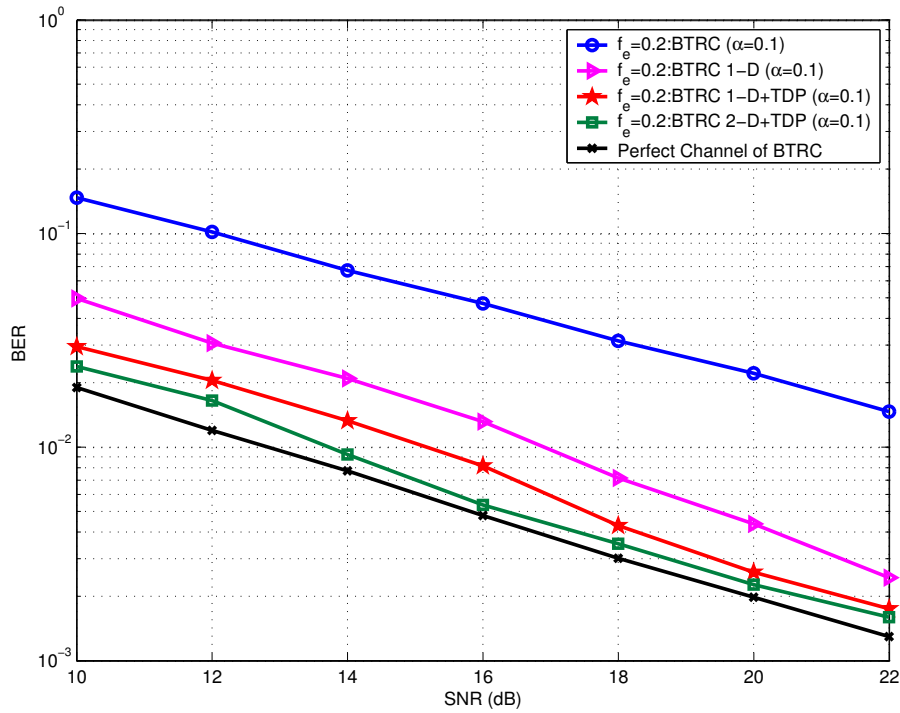
Figure 3.19: Effect of channel estimate on the SISO-OFDM system's BER performance.
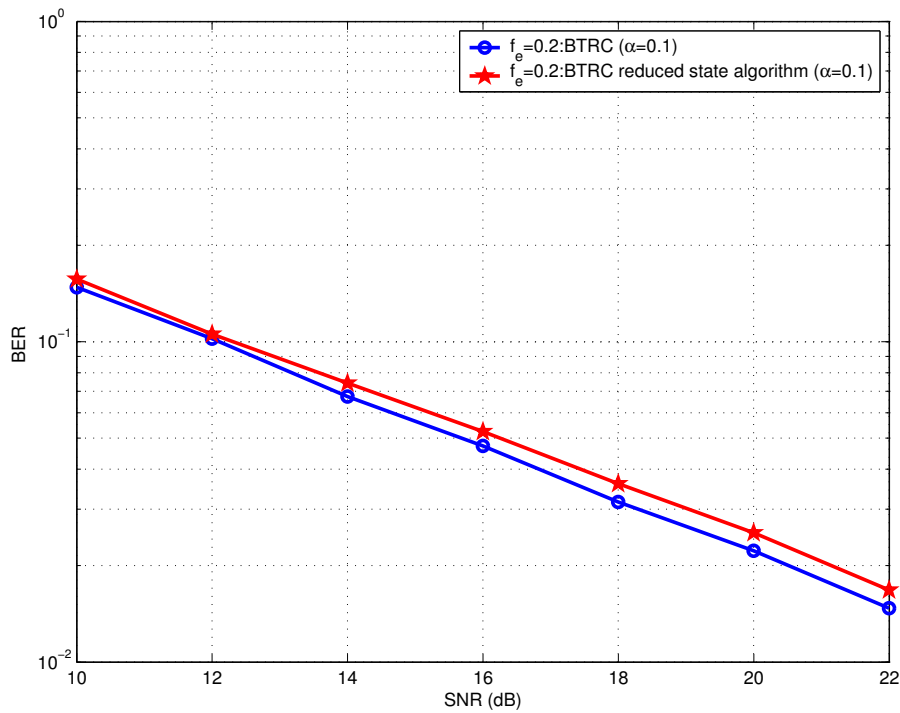
Figure 3.20: BER performance of SISO-OFDM systems using iterative joint FDC estimate with reduced-state DF method in Rayleigh fading channels.

Chapter 4

Joint Estimation for MIMO-OFDM Systems

4.1 Introduction

The efficiency of a communication system is often judged by how the main resources–power and signal dimensionality–is used. Until recently, the latter is measured by the time-bandwidth product of the transmitted waveform. By exploiting the degrees of freedom of the spatial domain, one is able to significantly increase the capacity of a wireless system [26] [27]. The spatial degrees of freedom is realized by using multiple antennas at both transmitter and receiver, generally referred to as the multiple-input multiple-output (MIMO) technologies.

The high spectral efficiency associated with a MIMO channel is achieved under the assumption that a richly scattering environment renders independent propagation paths between each pair of transmit and receive antennas. In a MIMO system, high-rate data transmission is accomplished by de-multiplexing, i.e., dividing the original data stream into several parallel data substreams, each of which is transmitted from a corresponding transmit antenna. All data substreams are independent of each other and different data substreams will result in co-antenna interference (CAI) upon reception. A well-known realization is the BLAST (Bell Labs Layered Space Time) system [28] that achieves high peak throughput with small constellations.

The OFDM scheme has been adopted by the wireless local-area-network (WLAN) standards IEEE 802.11a and 802.11g due to its high spectral efficiency and ability to combat frequency selective fading and narrowband interference. Thus if CAI can be mitigated, a MIMO-OFDM system can provide both high data rates and improved system performance through the use of the antenna as well as the frequency diversities.

Since the throughput enhancement of MIMO is especially high in richly-scattered scenarios of which indoor environments are typical examples, the widespread indoor deployments of WLAN systems makes MIMO-OFDM a strong and natural candidate for high throughput extension (802.11n) of the current WLAN standards.

This chapter examines the most critical design issue associated with a MIMO-OFDM system, namely, the problem of frequency compensation, channel estimation and data detection. We will explain why it is possible and indeed feasible to extend the joint FDC estimation algorithm we presented in the last chapter to a MIMO-OFDM environment.

4.2 System Model

Consider a MIMO system with M_T transmit antennas and M_R receive antennas. Assuming a flat block-fading channel model, we can express the equivalent signal part of the received time-domain samples at qth receive antenna as

$$b^q[n] = \sum_{p=1}^{M_T} \tilde{s}^{q,p}[n], \quad q = 1, 2, \ldots, M_R. \tag{4.1}$$

where

$$\tilde{s}^{q,p}[n] = \frac{1}{N} \sum_{k=0}^{N-1} \sqrt{\frac{E_s}{M_T}} a_k^p H_k^{q,p} e^{j2\pi nk/N} e^{j2\pi f_e n/N} \tag{4.2}$$

corresponds to the OFDM signal sent from the pth transmit antenna to the qth receive antenna. Moreover,

- a_k^p represents the symbol carried by the kth subcarrier at the pth transmit antenna,

- $H_k^{q,p}$ is the kth subcarrier's channel transfer function between the qth receive antenna and the pth transmit antenna,

- E_s is the average energy allocated to the kth subcarrier across the transmit antennas,

- f_e is the CFO normalized by the inter-carrier spacing, and

- N is the total number of sub-carriers for each transmit antenna.

After establishing proper frame (symbol) timing, removing the cyclic prefix and taking FFT on the time-domain samples, the received baseband frequency domain signal at the qth RX antenna reads

$$
\begin{aligned}
r_k^q &= \sum_{n=0}^{N-1} \tilde{b}^q[n] e^{-j2\pi nk/N} + n_k^q \\
&= \sum_{p=1}^{M_T} \sum_{m=0}^{N-1} a_m^p H_m^{q,p} W_{k-m}^{f_e} + n_k^q \\
&= \sum_{p=1}^{M_T} y_k(f_e, \mathbf{a}^p, \mathbf{H}^{q,p}) + n_k^q, \quad q = 1, 2, \ldots, M_R.
\end{aligned}
\tag{4.3}
$$

where $\tilde{b}^q[n]$ is the "folding window signal" from all transmit antennas.

Fig. 4.1 plots the transmission channel model for the qth receive antenna with respect to M_T transmit antennas. Comparing the above equation with (2.13), we find that to apply the joint FDC method to solve (4.3), we will have a trellis with the number of trellis states equals to M^{2L*M_T} since we now have to consider all transmitted data streams from all transmit antennas.

4.3 MIMO-OFDM Channel Estimation

Rewriting (4.3) in matrix form (for qth RX antenna)

$$
\begin{bmatrix} r_0^q \\ r_1^q \\ \vdots \\ r_{N-1}^q \end{bmatrix} = \begin{bmatrix} W_0^{f_e} & \cdots & W_{-N+1}^{f_e} \\ \vdots & \ddots & \vdots \\ W_{N-1}^{f_e} & \cdots & W_0^{f_e} \end{bmatrix} \begin{bmatrix} \sum_{p=1}^{M_T} H_0^{q,p} a_0^p \\ \sum_{p=1}^{M_T} H_1^{q,p} a_1^p \\ \vdots \\ \sum_{p=1}^{M_T} H_{N-1}^{q,p} a_{N-1}^p \end{bmatrix} + \begin{bmatrix} n_0^q \\ n_1^q \\ \vdots \\ n_{N-1}^q \end{bmatrix}
\tag{4.4}
$$
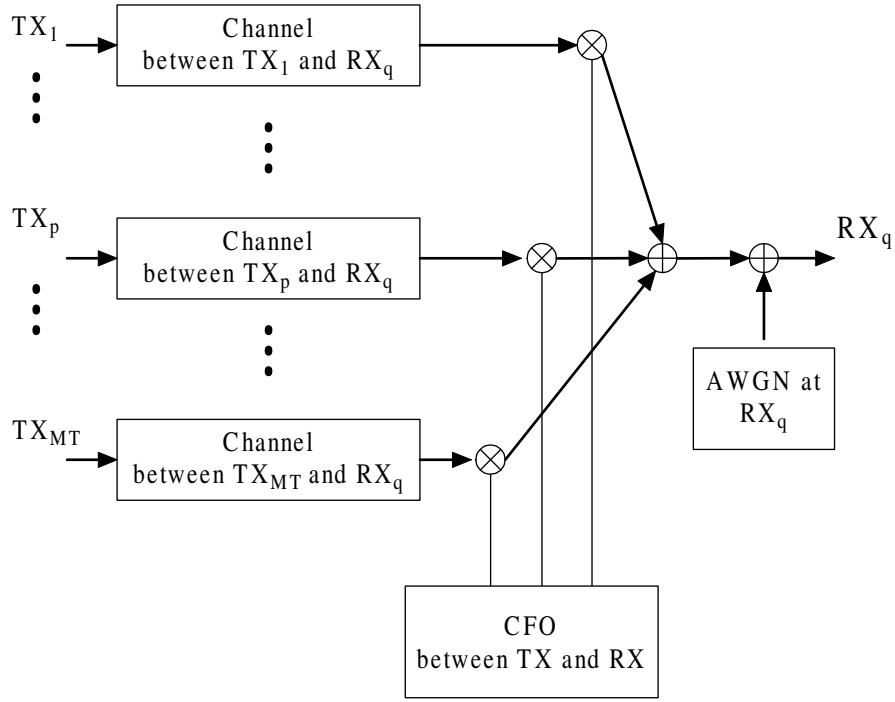
Figure 4.1: Channel model for the qth receive antenna.

and invoking the substitutions,

$$\mathbf{r}^q = [r_0^q \ r_1^q \ \cdots \ r_{N-1}^q]^T \tag{4.5}$$

$$\mathbf{n} = [n_0^q \ n_1^q \ \cdots \ n_{N-1}^q]^T \tag{4.6}$$

$$\mathbf{H}_A^q = [(\mathbf{H}_A^q)_0 \ (\mathbf{H}_A^q)_1 \ \cdots \ (\mathbf{H}_A^q)_{N-1}]^T \tag{4.7}$$

$$= \left[\sum_{p=1}^{M_T} H_0^{q,p} a_0^p \ \sum_{p=1}^{M_T} H_1^{q,p} a_1^p \ \cdots \ \sum_{p=1}^{M_T} H_{N-1}^{q,p} a_{N-1}^p \right]^T \tag{4.8}$$

$$\mathbf{F} = \begin{bmatrix} W_0^{f_e} & \cdots & W_{-N+1}^{f_e} \\ \vdots & \ddots & \vdots \\ W_{N-1}^{f_e} & \cdots & W_0^{f_e} \end{bmatrix} \tag{4.9}$$

we obtain

$$\mathbf{r}^q = \mathbf{F}\mathbf{H}_A^q + \mathbf{n}. \tag{4.10}$$

48

Assuming the data sequence and the CFO are known, we first compensate for the CFO through the LS estimate

$$
\begin{aligned}
\widehat{\mathbf{H}}_A^q &= \left[(\widehat{\mathbf{H}}_A^q)_1 \ (\widehat{\mathbf{H}}_A^q)_2 \ \cdots \ (\widehat{\mathbf{H}}_A^q)_{N-1} \right]^T \\
&= (\mathbf{F}^H \mathbf{F})^{-1} \mathbf{F}^H \mathbf{r}^q
\end{aligned}
\tag{4.11}
$$

The kth subcarrier over M_R receive antennas reads

$$
(\widehat{\mathbf{H}}_A)_{k,t} = \left[(\widehat{\mathbf{H}}_A^1)_{k,t} \ (\widehat{\mathbf{H}}_A^2)_{k,t} \ \cdots (\widehat{\mathbf{H}}_A^{M_R})_{k,t} \right]^T
\tag{4.12}
$$

$$
\mathbf{A}_{k,t} = [a_{k,t}^1 \ a_{k,t}^2 \ \cdots \ a_{k,t}^{M_T}]^T
\tag{4.13}
$$

where the index $1 \le t \le M$ denotes the tth OFDM symbol of an M-symbol block that suffer from the same flat (block-)fading.

Stacking up the M received frequency domain symbols we have

$$
\overline{(\widehat{\mathbf{H}}_A)_k} = \widehat{\mathbf{H}}_k \overline{\mathbf{A}}_k
\tag{4.14}
$$

where

$$
\overline{(\widehat{\mathbf{H}}_A)_k} = [(\widehat{\mathbf{H}}_A)_{k,1} \ (\widehat{\mathbf{H}}_A)_{k,2} \ \cdots \ (\widehat{\mathbf{H}}_A)_{k,M}]
$$

$$
\overline{\mathbf{A}}_k = [\mathbf{A}_{k,1}, \mathbf{A}_{k,2}, \cdots, \mathbf{A}_{k,M}]
\tag{4.15}
$$

and $\widehat{\mathbf{H}}_k$ is the $M_R \times M_T$ complex channel matrix for the kth subcarrier.

Finally, the channel matrix can be estimated by

$$
\widehat{\mathbf{H}}_k = \overline{(\widehat{\mathbf{H}}_A)_k} \ \overline{\mathbf{A}}_k^H (\overline{\mathbf{A}}_k \overline{\mathbf{A}}_k^H)^{-1}
\tag{4.16}
$$

on the premise that the rank of $\overline{\mathbf{A}}_k$, the "over symbols data matrix at subcarrier k" is greater than M_T. In other words, one has to sent at least M_T OFDM symbols over the same flat fading block (a coherent time) in order to obtain a proper channel estimate [29].

4.4 An Iterative Joint FDC Estimation Algorithm

Based on the above discussion, we suggest an iterative joint FDC estimation algorithm as follows.

C.1 (Channel estimate initialization) Set $\widehat{\mathbf{H}}_O$ to be the channel estimate from the previous OFDM symbols.

C.2 (Frequency Estimate Initialization) Set the initial estimate $\hat{f}_e = 0$.

C.3 (Starting the FD iteration loop) Use current channel estimate for the frequency-data sequence iteration loop. Calculate the channel frequency response compensation matrix $\mathbf{F} = [W_k^{f_e}]$ based on (4.9) and current frequency estimate $\hat{f}_e$.

C.4 (Compute the tentative data estimate) Given the observed sample vector $\mathbf{r}$ defined by (4.5), perform the Viterbi algorithm with the branch metric

$$\lambda_k^q = \left| r_k^q - \sum_{p=1}^{MT} y_k(\hat{f}_e, \mathbf{a}^p, \widehat{\mathbf{H}}^{q,p}) \right|^2 \tag{4.17}$$

to find a conditional optimal data sequence estimate $\hat{\mathbf{a}}$

C.5 (Update the frequency estimate) Update the CFO estimate by minimizing the cost function :

$$C = \sum_q \sum_k \left| r_k^q - \sum_{p=1}^{MT} y_k(f_e, \hat{\mathbf{a}}^p, \mathbf{H}^{q,p}) \right|^2 \tag{4.18}$$

C.6 (Convergence check and end of the FD loop) If the new CFO estimate $\hat{f}_e$ is close to the previous estimate, i.e. absolute difference is less than 10^{-6}, then stop the current FD iteration and release the new estimates $\hat{\mathbf{a}}$ and $\hat{f}_e$; otherwise go back to Step 3.

C.7 (Channel estimate update) Compute a new channel estimate $\widehat{\mathbf{H}}_N$ using (4.16) based on the current estimates $\hat{f}_e$ and $\hat{\mathbf{a}}$.

C.8 (Convergence check for the channel estimate) If the new channel estimate $\widehat{\mathbf{H}}_N$ is close enough to the previous estimate, more specifically, if

$$\left| \frac{\hat{H}_N - \hat{H}_O}{\hat{H}_N} \right|^2 < 10^{-2}$$

then stop iteration and release the most recent estimates. Otherwise, go to Step 3.

4.5 Numerical Experiments

The simulation parameters and environments used in the following paragraphs are identical to those used in the SISO-OFDM system simulations, except that we now have $M_T \times M_R$ independent channels. The BER performance of the iterative joint FDC estimation algorithm for the 2×2 configuration is given in **Fig. 4.2**. For comparison purpose the SISO performance curve is shown in the same figure. Clearly, the spatial diversity does pay off–with a gain of more than 4 dB for BER $< 10^{-2}$. The MSEE performance of the corresponding frequency estimate is plotted in **Fig. 4.3**. Similarly, we find that more receive antennas leads to better performance due to the MIMO diversity gain. **Fig. 4.4** shows the effect of the channel estimate on the BER performance. These curves indicate that, as expected, the model-based channel estimation still outperform the LS channel estimate for MIMO-OFDM systems.
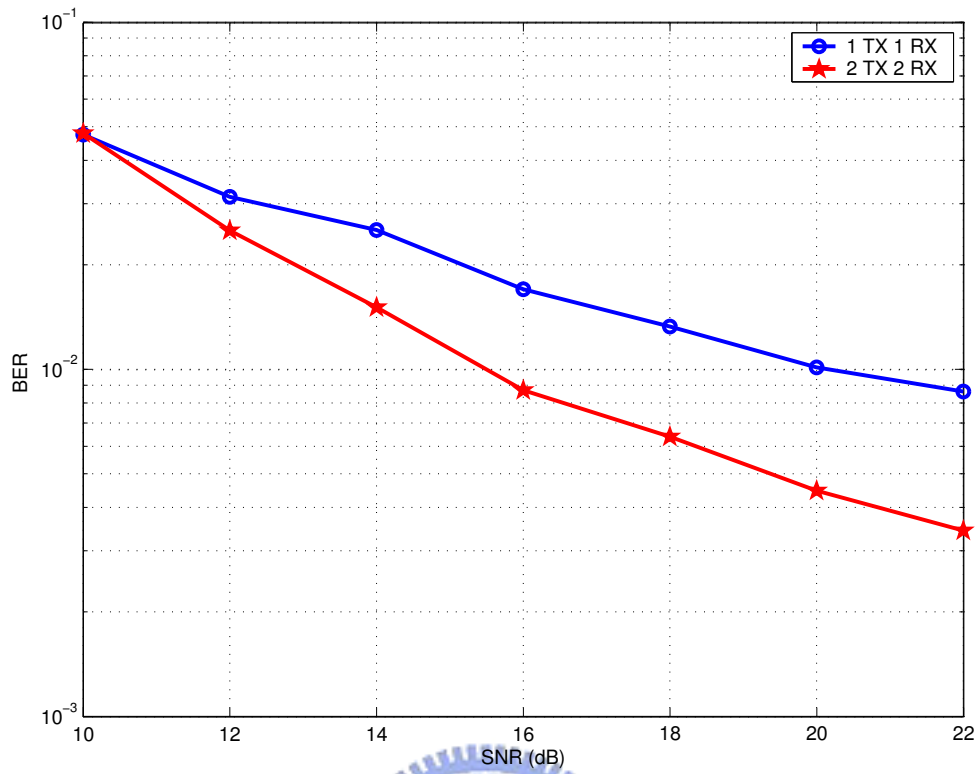
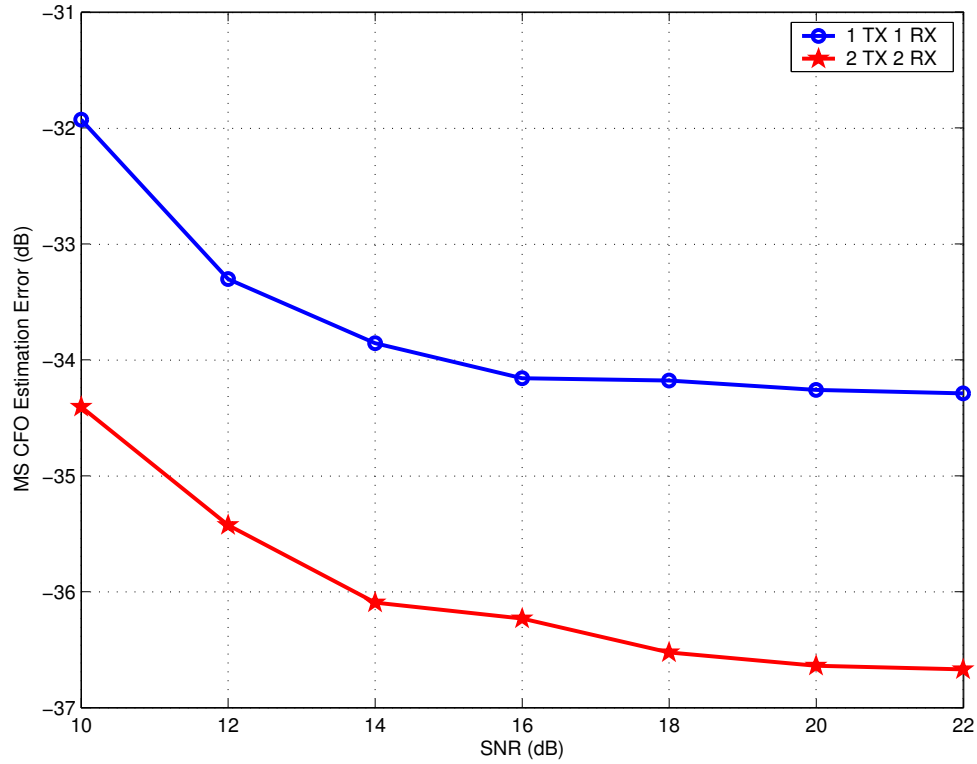Figure 4.2: BER performance of MIMO- and SISO-OFDM systems using iterative joint FDC estimate ($f_e = 0.2$).

Figure 4.3: MSEE performance of CFO estimates in MIMO-OFDM systems for 2×2 and SISO configurations ($f_e = 0.2$).
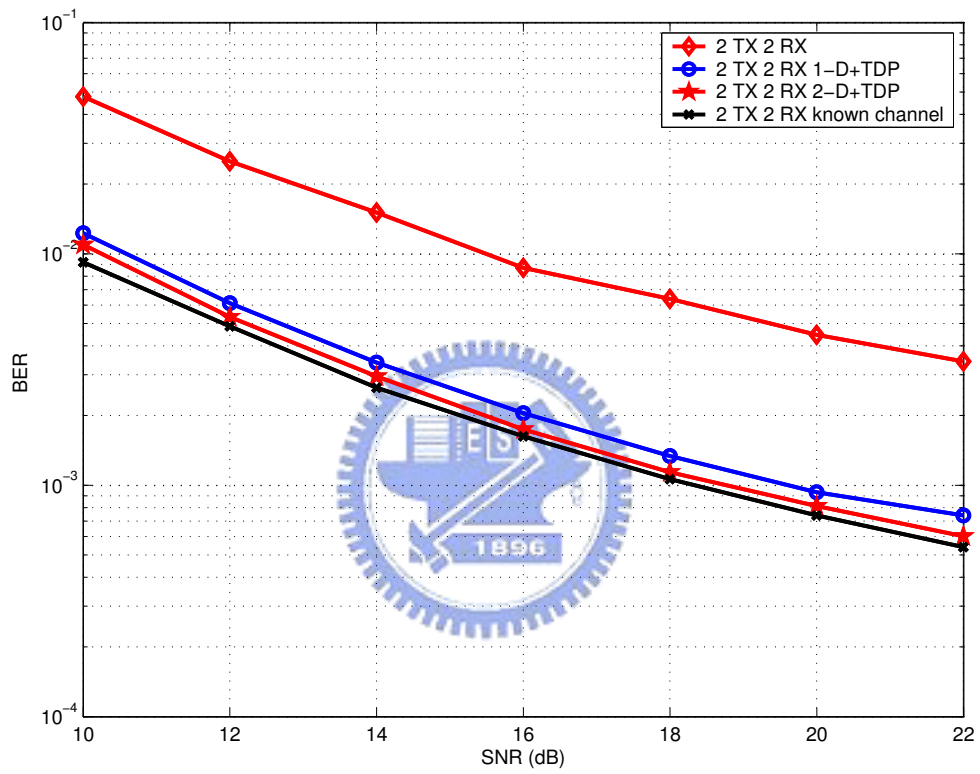
Figure 4.4: Effect of the channel estimate on the MIMO-OFDM system's BER performance ($f_e = 0.2$).

Chapter 5

Conclusion

We have presented iterative joint estimation and detection algorithms for OFDM systems in various scenarios. An iterative joint frequency estimation and data sequence detection algorithm is first given for AWGN channels. By incorporating a proper channel estimation method, we then provide an iterative joint FDC estimation algorithm for SISO-OFDM systems. Some refinements for enhanced performance and complexity reduction are suggested. Finally, we extend the our joint FDC estimation algorithm to MIMO-OFDM environments. Simulation based on a candidate IEEE 802.11n standard– the Tgn Sync (Task Group n) proposal–is provided to validate various joint estimation and detection algorithms. The corresponding numerical results do prove that the proposed solutions are both practical under the assumed channel conditions. Our solution can operate in the blind mode if the initial CFO is less than half of a subcarrier spacing. Otherwise, we can use the preamble (like the 802.11n case) to reduce the CFO to within the desired range. Our proposal can then be used for subsequent data detection and CFO/channel tracking in time-varying channels.

Appendix A

802.11n PHY Specification

For convenience of reference, we present in this appendix some signal specifications of the 802.11n standard that are used in our simulation.

A.1 MIMO data path overview

The general data path for MIMO transmission is shown in **Figure. A.1** The FEC
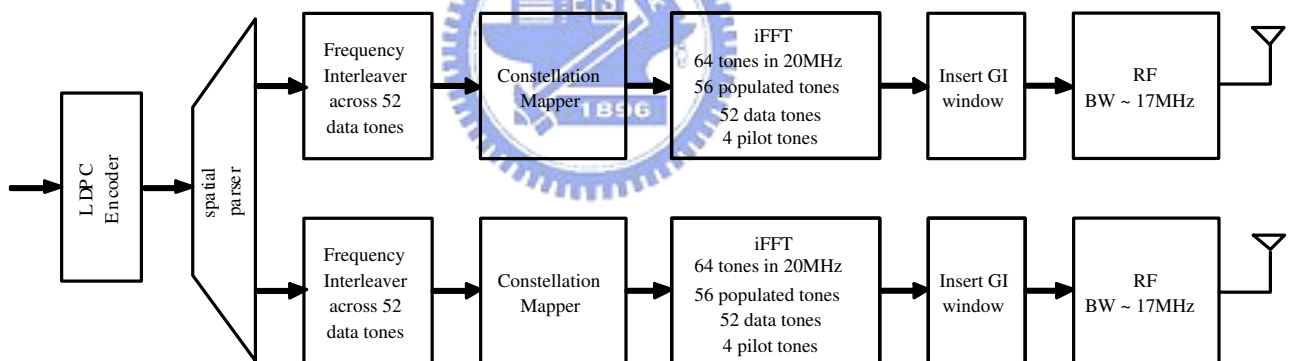
Figure A.1: The MIMO datapath of the IEEE 802.11n standard.

architecture has a single encoder. For the convolutional code (CC), the mother code is rate 1/2 with industry-standard generator polynomials, $g_0 = 133_8$ and $g_1 = 171_8$. Encoded bits may be punctured to produce code rates 2/3, 3/4 or 5/6. For the LDPC code different code rates are produced within the encoder and external puncturing is not applied. Processing of bits following encoding/puncturing is identical for both CC and LDPC.

The punctured bits are then distributed to N_{SS} spatial streams via the spatial stream parser. For each spatial stream, blocks of bits that map to a single OFDM symbol are interleaved.

Interleaved bits are then mapped to QAM constellation points. The mapping may be BPSK, QPSK, 16 QAM, 64 QAM or 256 QAM.

The next step is the antenna map transformation. This transformation maps N_{SS} spatial streams to N_{T_x} transmit antenna streams.

After the antenna map, antenna streams are transformed to the time domain via the IFFT. The cyclically extended GI (guard interval) is added. Finally, time domain windowing (not shown) is applied to create a continuous time-domain signal, and analog and RF processing yields the signals that are applied to transmit antennas.

A.2 High Throughput (HT) PHY layer convergence protocol (PLCP) preamble

The functions performed by the preamble include:

1. Start-of-Packet (SoP) detection

2. Automatic gain control (AGC)

3. Coarse Frequency Offset Estimation

4. Coarse Timing Offset Estimation

5. Fine Timing Offset Estimation

6. Fine Frequency Offset Estimation

7. Channel Estimation

The HT preamble in our proposal is a concatenation of the legacy preamble (identical to 802.11a/g) and a HT-specific preamble, as shown in **Figure A.2**: Concatenation of
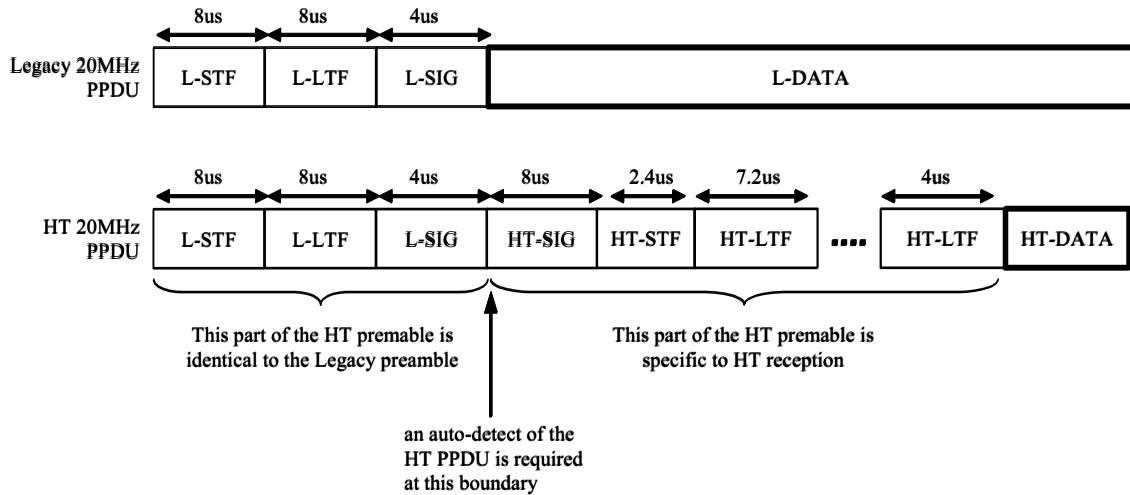
56

Figure A.2: HT Preamble format

the legacy preamble allows PHY layer interoperability with 802.11a and extended rate PHY (ERP)-802.11g modems.

A HT receiver does not know a priori whether it is receiving a legacy PHY protocol data unit (PPDU) or a HT PPDU. Hence, a HT receiver has to perform an auto-detect after the legacy signal field (L-SIG) as to whether a HT-SIG is being received or legacy data (L-DATA). Our preamble format includes two provisions for auto-detecting the HT-SIG: (a) transmitting the HT-SIG as a BPSK signal on the quadrature axis instead of the in-phase axis, and (b) inverting the pilot polarity in going from the L-SIG to the HT-SIG.

The legacy part of the HT preamble allows a legacy receiver to properly decode the L-SIG. A HT receiver shall also perform functions 1 through 7 (SoP to Channel Estimation) to successfully decode the HT-SIG. It is anticipated that functions 1 through 4 (and perhaps function 5) are performed by the legacy short training field (L-STF), and functions 5 through 7 are performed by the legacy long training field (L-LTF).

Since a HT device (in our proposal) shall support multiple transmit antennas, the legacy part of the preamble can either be transmitted from one antenna or from multiple antennas. If more than one antenna is used for transmission, it is recommended that the

signal be shifted in a cyclical fashion across the transmit antenna array. This technique introduces cyclical delay diversity (CDD), and it tends to reduce the "effective" length of the guard interval, as seen by a legacy device. Hence, the total shift across the transmit antenna array should be limited to 50ns.

A.3 Basic MIMO PPDU format

The HT Physical layer defines a PPDU format that provides interoperability and coexistence with 802.11a stations and with ERP-OFDM stations of 802.11g at the link level without protection mechanisms. **Figure A.3** shows the PPDU format for the basic MIMO mode:
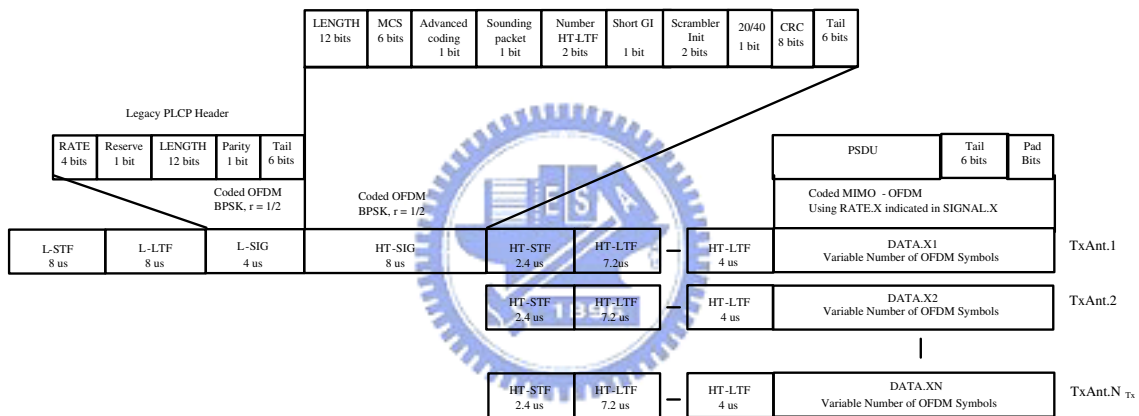

Figure A.3: HT Preamble format

L-STF is the Legacy Short Training Field. L-LTF stands for Legacy Long Training Field. L-SIG is based on the Legacy SIGNAL field.

The HT-SIG field is the signal field dedicated to the HT mode. The structure of this field is the same as the L-SIG. Since our proposal supports interoperability between HT devices and legacy OFDM devices at the PHY layer, a HT receiver will not know a priori whether a legacy packet or an HT packet is being received. That determination can only be made after the L-SIG. Our proposal supports two mechanisms for signaling a HT transmission: (a) send the HT-SIG as a BPSK signal on the quadrature axis, instead of on the in-phase axis, and (b) invert the polarity of the pilots in the HT-SIG

with respect to the pilots in the L-SIG. These two mechanism allow an auto-detect of a HT transmission. Note that the pilots in the HT-SIG are not transmitted on the Quadrature axis.

Bibliography

[1] ETSI, "Radio broadcasting systems: Digital Audio Broadcasting to mobile, portable and fixed receivers," *European Telecommunication Standard,* ETS 300 401 v1.3.2, Sep. 2000.

[2] ETSI, "Digital Video Broadcasting: framing structure, channel coding, and modulation for digital terrestrial telwisio," *European Telecommunication Standard,* ETS 300 744 v1.3.1, Aug. 2000.

[3] H. Sari, G. Karam, and I. Jeanclaude, "Transmission techniques for digital terrestrial TV Broadcasting," *IEEE Commun. Mag.,* vol. 33, pp. 100-109, Feb. 1995.

[4] ETSI, "Digital Video Broadcasting (DVB): Framing structure, channel coding and modulation for digital terrestrial television (DVB-T)," *European Telecommunication Standard,* ETS 300 744, Aug. 1997.

[5] Broadband Radio Access Networks (BRAN); High Performance Radio Local Area Networks (HIPERLAN) Type 2, System Overview, ETSI TR 101 683, v0.1.2, 1999.

[6] IEEE, "Part II: Wireless LAN Medium Access Control (MAC) and Physical Layer (PHY) Specifications: High Speed Physical Layer in the 5-GHn Band," *IEEE Std.,* 802.11a-1999, Sept. 1999.

[7] "High throughput extension to the 802.11 standard," WWiSE, Aug. 2004.

[8] "TGn Sync proposal technical specification," TGn Sync, Aug. 2004.

[9] T. Pollet, M. Van Bladel, and M. Moeneclaey, "BER sensitivity of OFDM systems to carrier frequency offset and Wiener phase noise," *IEEE Trans. Commun.*, vol. 43, pp. 191 - 193, Feb./Mar./Apr. 1995.

[10] P.-H. Moose, "A technique for orthogonal frequency-division multiplexing frequency offset correction," *IEEE. Trans. Commun.*, vol. 42, pp. 2908-2914, Oct. 1994.

[11] H. Bolcskei, "Blind estimation of symbol timing and carrier frequency offset in wireless OFDM systems," *IEEE Trans. Commun.*, vol. 49, pp. 988-999, June 2001.

[12] H. Jin and J. Moon, "Joint CFO, Data Symbol and Channel Response Estimation in OFDM Systems," *IEEE ICC 2005*, Seoul, Korea, May 2005.

[13] H. Sari, G. Karam, and I. Jeanclaude, "Transmission techniques for digital terrestrial TV broadcasting," *IEEE Commun. Mag.*, vol. 33, pp. 100-109, 1995.

[14] C. Muschalik, "Improving an OFDM Reception Using an Adaptive Nyquist Windowing ," *IEEE Trans. Commun.*, vol. 19, pp. 628-634, Oct. 1971.

[15] P. Tan and N.C. Beaulieu, "A Novel Pulse-Shaping for Reduced ICI in OFDM Systems ," *IEEE Vehicular Technology Conf.* - Fall, Los Angeles, pp. 456-459, Sept. 26-29, 2004.

[16] R. Li and G. Stette, "Waveform Shaped MCM for Digital Microwave Radio," in *Proc. of IEEE ICC'95,* Seattle, Washington, USA, pp. 1695-1699, June 1995,

[17] A. Vahlin and N. Holte, "Optimal Finite Duration Pulses for OFDM," *IEEE Trans. Commun.,* vol. 44, pp.10-14, 1996.

[18] S. Muller-Weinfurtner and J. Huber, "Optimum Nyquist Windowing for Improved OFDM Receivers," in *Proc. IEEE Global Telecommunications. Conf.,* vol. 44, pp.711-715, Nov. 2000.

[19] A.-V. Oppenheim, Ronald W. Schafer, *Discrete-Time Signal Processing* Second Edition.

[20] Arthur J Redfern, "Receiver Window Design for Multicarrier Communication Systems," *IEEE Journal on Selected Areas in Commun.,* vol.20, pp 1029-1036, June 2002.

[21] Dan Zhang, Pigyi Fan, Zhigang Cao, "Receiver window design for narrowband interference suppression in IEEE 802.11a system," *IEEE Commun., 2004 and the 5th Intern. Symposium on Multi-Dimensional Mobile Commun. Proc. ,* vol.2, pp.839-842, Sept. 2004

[22] A. Duel-Hallen and C. Heegard, "Delayed decision-feedback sequence estimation," *IEEE Trans. Commun.,* vol. 37, pp. 428-436, May 1989.

[23] W. C. Jakes, Jr., Ed., "Microwave mobile communications" *New York: Wiley,* Jun. 1974.

[24] M. X. Chang and Y. T. Su, "Model-based channel estimation for OFDM signals in Rayleigh fading," *IEEE Trans. Commun.,* vol. 50, pp. 540-544, Apr. 2002.

[25] Y. Zhao and A. Huang, "A novel channel estimation method for OFDM communization systems based on pilot signals and transform-domain processing," in *Proc. IEEE 47th Vech. Tech. Conf.,*Phoenix, USA, pp. 2089-2093, May 1997.

[26] G. J. Foschini and M. J. Gans, "On limits of wireless communications in a fading environment when using multiple antennas," *Wireless Personal Communications,* pp. 311-335, 1998.

[27] E. Telatar, "Capacity of multi-antenna Gaussian channels," *European Trans. on Telecommunications,* vol. 10, pp. 585-596, 1999.

[28] G. D. Golden, C. J. Foschini, and P. W. Wolniansky, "Detection algorithm and initial laboratory results using V-BLAST space-time communication architecture," *Electronics Letters,* vol. 35, pp. 14-16, 1999.

[29] M. Biguesh and A. B. Gershman," MIMO channel estimation: optimal training and tradeoffs between estimation techniques," *2004 IEEE Intern. Conf. on Commun.* vol. 5, pp. 2658-2662, June 2004.

簡　　歷

姓　　　名：呂子逸

居　住　地：桃園縣

出生年月日：民國七十年五月三十一日

興趣 ：旅遊、籃球、撞球、游泳

學　經　歷：

　　　武陵高中　　　　　　（85 年 9 月～88 年 6 月）

　　　交通大學電信工程學系大學部　　（88 年 9 月～92 年 6 月）

　　　交通大學電信工程學系碩士班　（92 年 9 月～94 年 7 月）

Graduate Course：

Digital Communication
Random Process
Digital Signal Processing
Detection and Estimation Theory
Digital Communication Receiver
Adaptive Signal Processing
Soft-Decision Decoding of Linear Codes
Design of Communication System VLSI Chips and Circuits